Towards Accurate Density and Interfacial Tension Modeling for Carbon Dioxide/Water Mixtures

by

Zixuan Cui

A thesis submitted in partial fulfillment of the requirements for the degree of

Master of Science

in

Petroleum Engineering

Department of Civil and Environmental Engineering

University of Alberta

ABSTRACT

Phase behavior of carbon dioxide/water (CO_2/H_2O) binary mixtures plays an important role in various CO_2-based industry processes, including CO_2 injection for enhanced oil recovery and CO_2 storage in saline aquifers. Engineering design of such processes requires an appropriate thermodynamic model that can well capture the vapor-liquid equilibria (VLE), liquid-liquid equilibria (LLE), phase densities, and interfacial tension (IFT) of CO_2/H_2O mixtures. This work aims to screen such a model out of a number of promising candidate models. A special attention is given towards the phase density predictions as well as IFT predictions. A comprehensive analysis reveals that Peng-Robinson Equation of State (PR EOS) (Peng and Robinson, 1976), Twu α function (Twu *et al*., 1991), Huron-Vidal mixing rule (Huron and Vidal, 1979), and Abudour *et al.* (2013) volume translation model is the optimum model which yields average absolute percentage errors (abbreviated as *%AAD*) of 6.52% and 2.88% in reproducing the experimental phase composition data (i.e., 195 data points) and density data (i.e., 855 data points) collected in the literature over 278.00-478.35 K and 2.20-1291.90 bar. After reliable modeling of phase compositions and densities for CO_2/H_2O mixtures has been achieved with the optimal thermodynamic model, a new empirical IFT correlation for CO_2/H_2O mixtures is proposed through a nonlinear regression of the measured IFT data collected from the literature over 278.15-477.59 K and 1.00-1200.96 bar (i.e., a total of 778 data points for CO_2/H_2O mixtures with 589 training data and 189 test data). The inputs of the IFT model are the phase compositions and densities calculated by the aforementioned PR EOS model. Although the newly proposed IFT correlation only slightly improves the prediction accuracy yielded by the refitted Chen and Yang's correlation (Chen and Yang, 2019), the proposed empirical correlation avoids the inconsistent prediction trend present in Chen and Yang's model (Chen and Yang, 2019) and yields smooth IFT predictions.

ACKNOWLEDGMENTS

I would like to express my sincere gratitude to my supervisor, Dr. Huazhou Li, for his guidance and patience throughout my master program. He taught me not only the way to conduct quality research but also professional skills useful for my future career. In addition, I want to thank my examination committee chair, Dr. Zhehui Jin, and the examination committee members, Dr. Japan Trivedi and Dr. Alireza Nouri, for their critical and valuable comments. I also would like to express my sincere thanks to my family, my friends, as well as my colleagues in Dr. Li's research group. Finally, I greatly acknowledge a Petro-Canada Young Innovator Award from the University of Alberta to H. Li.

DEDICATION

This dissertation is dedicated to my dearest parents, Mr. Lizhu Cui and Mrs. Yansheng Guo.

TABLE OF CONTENTS

LIST OF TABLES

LIST OF FIGURES

CHAPTER 1 INTRODUCTION

1.1 Research Background

CO_2's interaction with H_2O is frequently seen in several subterranean processes (such as CO_2-based enhanced oil recovery and CO_2 storage). Phase behavior of CO_2/H_2O mixtures under subterranean conditions plays a great role in affecting the overall efficiency of these processes. Thus, how to accurately model the phase behavior of CO_2/H_2O mixtures, such as vapor-liquid equilibria (VLE), liquid-liquid equilibria (LLE), phase density, and IFT, becomes drastically important. Overall, an appropriate combination of cubic equation of state (CEOS), mixing rule in CEOS, α function, volume translation, and IFT model should be determined to well capture the VLE/LLE, phase density, and IFT of CO_2/H_2O mixtures.

1.2 Literature Review of Existing VLE/LLE, Volume Translation and IFT Models

1.2.1 Thermodynamic Models for Predicting VLE/LLE of H_2O/CO_2 Binary Mixtures

Due to their simplicity and good reliability, CEOSs such as SRK EOS[1] and PR EOS[2] are the most widely used thermodynamic models for the phase behavior modeling of CO_2/H_2O binary mixtures[3-4]. Numerous articles have addressed phase-composition modeling of CO_2/H_2O mixtures. Two types of methods, ϕ-ϕ (fugacity-fugacity) approach and γ-ϕ (activity-fugacity) approach[5-6], are often applied in such modeling processes. Because γ-ϕ approach has a discontinuity issue in the phase diagram near the critical region[6], this work focuses on ϕ-ϕ based methods.

Pederson *et al*.[7] combined SRK EOS[1] with the Huron-Vidal mixing rule[8] in water-hydrocarbons systems. Their modeling results showed that with the consideration of excess Gibbs energy in the ϕ-ϕ based method, phase behavior of the mixtures containing water could be represented accurately.

Valtz *et al*.[9] found that the most accurate model is PR EOS[2], Mathias-Copeman α function[10], and Wong-Sandler mixing rule[11] with 5.4*%AAD* (average absolute percentage deviation) in reproducing the measured phase composition data for CO_2/H_2O mixtures. However, the temperature and pressure ranges used by Valtz *et al*.[9] were narrow (278.2-318.2 K and 4.64-79.63 bar, respectively). In addition, the parameters in Wong-Sandler mixing rule[11] are given as discrete values at different isotherms. Zhao *et al*.[6] applied PRSV EOS[12] and the Wong-Sandler mixing rule[11] to calculate phase compositions, obtaining 7.12*%AAD* in reproducing the measured phase-composition data of CO_2/H_2O mixtures over a wide range of temperatures and pressures. Similar to Valtz *et al*.[9]'s study, in the study by Zhao *et al*.[6], the parameters in the Wong-Sandler mixing rule[9] are provided as discrete values at different isotherms, instead of generalized correlations; their model is inconvenient to use since one has to make extrapolations based on the provided values when making predictions at conditions different from those given by Zhao *et al*.[6]. Abudour *et al*.[13] applied van der Waals (vdW) one-fluid mixing rule[14] with several temperature-dependent BIP correlations in PR EOS in determining phase compositions of CO_2/H_2O mixtures. With the tuned BIPs, their model yielded good accuracy (i.e., 5.0*%AAD*) in aqueous phase-composition predictions but lower accuracy (i.e., 13.0*%AAD*) in CO_2-rich phase-composition predictions.

A recent comprehensive study by Aasen *et al*.[3] revealed that the most accurate thermodynamic model (among the ones examined by them) in phase-composition and phase-density predictions for CO_2/H_2O mixtures is PR EOS[2], Twu α function[15], Huron-Vidal mixing rule[8], and constant volume translation. This model only yields 4.5%*AAD* in phase-composition calculations and 2.8*%AAD* in phase-density calculations for CO_2/H_2O mixtures. Aasen *et al*.[1], Valtz *et al*.[7], and Zhao *et al*.[4] also pointed out that more advanced models (e.g., the Cubic-Plus-Association (CPA)

EOS[16]) do not guarantee an improvement in the phase-composition predictions for CO_2/H_2O mixtures.

1.2.2 Volume Translation Models

With regards to phase-density calculations, CEOS based methods tend to overestimate liquid-phase molar volumes. A detailed discussion of this issue can be found in the studies by Matheis *et al.*[17] and Young *et al.*[18]. In order to address this problem, Martin[19] introduced the volume translation concept in CEOS to improve liquid-phase volumetric predictions. Peneloux *et al.*[20] developed volume translation schemes in SRK EOS[1] for pure substances. Jhaveri and Youngren[21] applied volume translation into PR EOS[2], leading to the improvement of liquid phase-density predictions. Volume translation method partially solves one inherent problem of CEOS, i.e., the inaccurate liquid density calculations. A thorough comparison of different types of volume translation methods can be found in Young *et al.*[18]'s work.

According to the study by Young *et al.*[18], the temperature-dependent volume translation method developed by Abudour *et al.*[22,23] provides the most accurate estimates on liquid-phase densities, although applying the temperature-pressure-dependent volume translation functions coupled with CEOS could potentially result in thermodynamic inconsistencies[22]. Aasen *et al.*[3] applied constant volume translation to phase-density calculations for CO_2/H_2O mixtures and achieved a significant improvement in density prediction accuracies. However, a more accurate volume translation function, the one proposed by Abudour *et al.*[22,23], was not applied in Aasen *et al.*[3]'s study; furthermore, it should be noted that Aasen *et al.*[3] used GERG-2008[24] and EOS-CG[25] calculated densities as reference densities instead of experimental data. In this study, we apply the volume translation method by Abudour *et al.*[22,23] to see if the use of this model can further improve phase-

density predictions for CO_2/H_2O mixtures; these predictions are compared to the measured density data documented in the literature.

1.2.3 IFT Correlations for CO_2/H_2O Mixtures

Parachor model[26] is one of the most widely applied models in predicting mixtures' IFT[27]. However, its accuracy heavily relies on the density difference between the two coexisting phases in a VLE or an LLE. Our experience in using Parachor model to calculate IFT of CO_2/H_2O mixtures shows that Parachor model is generally appropriate for the IFT estimation for VLE of CO_2/H_2O systems, but less suitable for the IFT estimation for LLE of CO_2/H_2O systems. This is primarily because an LLE of a CO_2/H_2O mixture has a smaller density difference than a VLE. Several empirical IFT correlations for CO_2/H_2O mixtures have been proposed in the literature. However, most of these correlations are only applicable to a limited temperature and pressure range[28].

In 2002, Hebach *et al*.[29] proposed a new correlation which correlated IFT with phase densities. Hebach *et al*.[29]'s model is suitable over a wide range of temperature and pressure conditions, although the prediction accuracy decreases with an increase in temperature or pressure. In 2019, Chen and Yang[30] proposed a new empirical IFT correlation for $CO_2/CH_4/H_2O$ ternary systems based on mutual solubility, and this model performs well for CO_2/H_2O binary mixtures. However, our experience in applying Chen and Yang's model shows that some breaking points can be observed in the predicted IFT curves under some conditions, hampering its ability in providing consistent and smooth IFT predictions. In addition, using two sets of BIPs (as applied in Chen and Yang[30]'s study) in the aqueous phase and non-aqueous phase can lead to thermodynamic inconsistency issue near the critical region as demonstrated by Li and Li[31].

1.2.4 Phase Behavior and IFT Modeling of CO_2/brine Mixtures

CO_2's interaction with brine is more commonly seen in subterranean processes compared with CO_2's interaction with pure water; therefore, numerous studies have focused on phase behavior modeling of CO_2/brine mixtures. CEOS based model is one of the most widely used methods for CO_2/brine phase behavior modeling[32].

In order to accurately model VLE/LLE of CO_2/brine mixtures, Søreide and Whitson[33] introduced a salinity term in the α function of PR EOS and implemented two sets of BIPs in the vdW mixing rule in the aqueous phase and the non-aqueous phase, yielding accurate phase-composition predictions for CO_2/brine, N_2/brine, and CH_4/brine mixtures. However, as discussed above, using two sets of BIPs can lead to thermodynamic inconsistency issue near the critical region[31]. In addition, only NaCl brine was considered in the study by Søreide and Whitson[33], other types of salts, such as $CaCl_2$ and KCl, were not included in their study.

Sørensen *et al*.[34] compared the performance of SRK EOS coupled with vdW mixing rule or Huron-Vidal mixing rule on VLE/LLE modeling of CO_2/brine mixtures over 298.15-523.15 K and 1-1400.31 bar. Three types of brine, NaCl, KCl, and $CaCl_2$, were selected and examined in their study. They pointed out that SRK EOS coupled with Huron-Vidal mixing rule is the most accurate model in phase-composition calculations for CO_2/brine mixtures. However, parameters in Huron-Vidal mixing rule are set as constants instead of generalized correlations in the work by Sørensen *et al*.[34], resulting in larger *%AAD*s in some systems (i.e., 20.3*%AAD* in CO_2/NaCl brine vs. 3.2*%AAD* in CO_2/KCl brine).

Yan and Chen[35] coupled PC-SAFT EOS[36] with electrolyte non-random two-liquid (eNRTL) activity coefficient model[37] to calculate CO_2 solubility in NaCl and Na_2SO_4 brine over 273.15-473.15 K and 0.075-1500 bar, yielding 14.1*%AAD* in reproducing the measured phase-composition data. However, compared with CEOS model, PC-SAFT model is more complex to use; besides, the prediction accuracy yielded by PC-SAFT model was only slightly better than that yielded by SRK EOS with Huron-Vidal mixing rule.

In terms of phase-density calculations, most research focuses on the development of empirical correlations to calculate aqueous-phase densities for CO_2/brine mixtures. A comprehensive investigation of these correlations can be found in the study by Hu *et al*.[32]. Although numerous studies have investigated the effect of volume translation in liquid-phase-density predictions in different systems (e.g. CO_2/H_2O, CO_2/crude oil), the effect of volume translation in phase-density predictions for CO_2/brine systems has not been well studied yet.

As for IFT modeling of CO_2/brine systems, several empirical IFT correlations for CO_2/brine mixtures have been proposed in the literature. However, most of these correlations are only applicable to a limited temperature and pressure range[28]. Zhang *et al*.[28] used neural networks to predict IFT of CO_2/brine mixtures. However, compared with empirical correlations, neural network models are less reliable to use; besides, our experience in using neural network model shows that neural network models can yield inconsistent IFT predictions due to the lack of enough training data. Chen and Yang's correlation[30] can be directly applied to CO_2/brine system since they took salinity into consideration in VLE/LLE calculations (i.e., introducing a salinity term in both α function and BIPs). However, their thermodynamic model bears inconsistency issue and yields

larger errors in phase-density calculations (although phase density is not included in their correlation).

Although the effect of salinity is not considered in this study, several modifications (e.g., refit the generalized correlations in Huron-Vidal mixing rule) could be implemented in the proposed modeling framework (e.g., PR EOS, Twu α function, Huron-Vidal mixing rule, and Abudour *et al*.[23] volume translation) to extend this thermodynamic model to the phase behavior modeling of CO_2/brine mixtures.

1.3 Problem Statement

The discussion above reveals that the previous studies on phase behavior modeling of the CO_2/H_2O mixtures tend to primarily focus on phase-composition modeling and pay less attention to phase-density calculations (especially for the CO_2-rich phase). Whereas, phase density is one important property in VLE and LLE since IFT calculations and flow simulations can heavily rely on such property. As for the IFT modeling, we are currently lacking a reliable IFT correlation that not only pays due tribute to the phase composition and density of CO_2/H_2O mixtures but also gives smooth and consistent IFT predictions over a wider range of temperature/pressure conditions.

1.4 Research Objectives

The main objective of this research is to achieve improved VLE/LLE, density, and IFT modeling for H_2O/CO_2 mixtures. The detailed objectives are as follows:

(1) To conduct a thorough literature review to screen the most promising thermodynamic models that can well capture the VLE and LLE of H_2O/CO_2 mixtures;

(2) To conduct phase-composition calculations by using PR EOS[2], Twu α function[15], and Huron-Vidal mixing rule[8] (as suggested by Aasen *et al*.[3]) and validate the accuracy of this

thermodynamic model by comparing the calculated phase compositions to the measured ones;

(3) To introduce Abudour *et al*.[23] volume translation model in phase-density calculations to check if applying this model can further improve the density-prediction accuracies;

(4) To propose a new IFT correlation for CO_2/H_2O mixtures based on the phase compositions and densities calculated by the aforementioned PR EOS models to yield more accurate and consistent IFT predictions.

1.5 Thesis Structure

This thesis is composed as follows:

(1) **Chapter 1** presents research background, literature review, problem statement, research objectives, and thesis structure.

(2) **Chapter 2** introduces the methodology employed in this thesis, including all the fundamental equations and models, empirical IFT correlations for CO_2/H_2O mixtures in previous studies, data collection and outlier detection method, and the new IFT correlation proposed in this study. This chapter also introduces the principle mechanisms of the non-linear regression algorithm as well as the two-phase flash calculations.

(3) **Chapter 3** demonstrates the performance of the optimal thermodynamic model in reproducing phase-composition and phase-density data, and the performance of the new empirical IFT correlation in IFT predictions. The thorough comparisons between the measured phase compositions, phase densities, and IFTs of CO_2/H_2O mixtures and the calculated ones from different models/correlations are also presented in this chapter.

(4) **Chapter 4** summarizes the conclusions obtained in this study and the recommendations for future work.

References

[1] Soave, G. Equilibrium constants from a modified Redlich-Kwong equation of state. *Chem. Eng. Sci*. **1972**, 27, 1197-1203.

[2] Peng, D.Y.; Robinson, D.B. A new two-constant equation of state. *Ind. Eng. Chem. Fundamen*. **1976**, 15, 59-64.

[3] Aasen, A.; Hammer, M.; Skaugen, G.; Jakobsen, J.P.; Wilhelmsen, Ø. Thermodynamic models to accurately describe the PVTxy-behavior of water/carbon dioxide mixtures. *Fluid Phase Equilib*. **2017**, 442, 125-139.

[4] Michelsen, M.L.; Mollerup, J.M. Thermodynamic models: fundamentals & computational aspects, second ed. Tie-Line Publications, 2007.

[5] Trusler, J.P.M. Thermophysical properties and phase behavior of fluids for application in carbon capture and storage processes. *Annu. Rev. Chem. Biomol. Eng*. **2017**, 8, 381-402.

[6] Zhao, H.; Lovo, S.N. Phase behavior of the CO_2-H_2O system at temperatures of 273-623 K and pressures of 0.1-200 MPa using Peng-Robinson-Stryjek-Vera equation of state with a modified Wong-Sandler mixing rule: an extension to the CO_2-CH_4-H_2O system. *Fluid Phase Equilib*. **2016**, 417, 96-108.

[7] Pedersen, K.S.; Milter, J.; Rasmussen, C.P. Mutual solubility of water and a reservoir fluid at high temperatures and pressures: experimental and simulated data. *Fluid Phase Equilib*. **2001**, 189, 85-97.

[8] Huron, M.J.; Vidal, J. New mixing rules in simple equations of state for representing vapor-liquid equilibria of strongly non-ideal mixtures. *Fluid Phase Equilib*. **1979**, 3, 255-271.

[9] Valtz, A.; Chaopy, A.; Coquelet, C.; Paricaud, P.; Richon, D. Vapor-liquid equilibria in the carbon dioxide-water system, measurement and modeling from 278.2 to 318.2 K. *Fluid Phase Equilib*. **2004**, 226, 333-344.

[10] Mathias, P.M.; Copeman, T.W. Extension of the Peng-Robinson equation of state to complex mixtures: evaluation of the various forms of the local composition concept. *Fluid Phase Equilib*. **1983**, 13, 91-108.

[11] Wong, D.S.H; Sandler, S.I. A theoretically correct mixing rule for cubic equations of state. *AIChE J*. **1992**, 38, 671-680.

[12] Stryjek, R.; Vera, J.H. PRSV: an improved Peng-Robinson equation of state for pure compounds and mixtures. *Can. J. Chem. Eng*. **1986**, 64, 323-333.

[13] Abudour, A.M.; Mohammad, S.A.; Gasem, K.A.M. Modeling high-pressure phase equilibria of coalbed gases/water mixtures with the Peng-Robinson equation of state. *Fluid Phase Equilib*. **2012**, 319, 77-89.

[14] van der Waals, J.D. Continuity of the gaseous and liquid state of matter. **1873**.

[15] Twu, C.H.; Bluck, D.; Cunningham, J.R.; Coon, J.E. A cubic equation of state with a new alpha function and a new mixing rule. *Fluid Phase Equilib*. **1991**, 69, 33-50.

[16] Kontogeorgis, G.M.; Voutsas, E.C.; Yakoumis, I.V.; Tassios, D.P. An equation of state for associating fluids. *Ind. Eng. Chem. Res*. **1996**, 35, 4310-4318.

[17] Matheis, J.; Müller, H.; Lenz, C.; Pfitzner, M.; Hickel, S. Volume translation methods for real-gas computational fluid dynamics simulations. *J. Supercrit. Fluids* **2016**, 107, 422-432.

[18] Young, A.F.; Pessoa, F.L.P.; Ahón, V.R.R. Comparison of volume translation and co-volume functions applied in the Peng-Robinson EoS for volumetric corrections. *Fluid Phase Equilib*. **2017**, 435, 73-87.

[19] Martin, J.J. Cubic equations of state—which? *Ind. Eng. Chem. Fundamen*. **1979**, 18, 81-97.

[20] Peneloux, A.; Rauzy, E.; Freze, R. A consistent correction for Redlich-Kwong-Soave volumes. *Fluid Phase Equilib*. **1982**, 8, 7-23.

[21] Jhaveri, B.S.; Youngren, G.K. Three-parameter modification of the Peng-Robinson equation of state to improve volumetric predictions. *SPE Res. Eng*. **1988**, 8, 1033-1040.

[22] Abudour, A.M.; Mohammad, S.A.; Robinson R.L.; Gasen, K.A.M. Volume-translated Peng-Robinson equation of state for saturated and single-phase liquid densities. *Fluid Phase Equilib*. **2012**, 335, 74-87.

[23] Abudour, A.M.; Mohammad, S.A.; Robinson R.L.; Gasen, K.A.M. Volume-translated Peng-Robinson equation of state for liquid densities of diverse binary mixtures. *Fluid Phase Equilib*. **2013**, 349, 37-55.

[24] Kunz, O.; Wagner, W. The GERG-2008 wide-range equation of state for natural gases and other mixtures: an expansion of GERG-2004. *J. Chem. Eng. Data*. **2012**, 57, 3032-3091.

[25] Gernert. J.; Span. R. EOS-CG: a Helmholtz energy mixture model for humid gases and CCS mixtures. *J. Chem. Thermodyn*. **2016**, 93, 274-293.

[26] Sugden, S. The Parachors and valency. 1930.

[27] Schechter, D.S.; Guo, B. Parachors based on modern physics and their uses in IFT prediction of reservoir fluids. *SPE Res. Eval. Eng*. **1998**, 1, 207-217.

[28] Zhang, J.; Feng, Q.; Wang, S.; Zhang, X.; Wang, S. Estimation of CO_2-brine interfacial tension using an artificial neural network. *J. Supercrit. Fluids* **2016**, 107, 31-37.

[29] Hebach, A.; Oberhof, A.; Dahmen, N.; Kögel, A.; Ederer, H.; Dinjus, E. Interfacial tension at elevated pressures – measurements and correlations in the water + carbon dioxide system. *J. Chem. Eng. Data*. **2002**, 47, 1540-1546.

[30] Chen, Z.; Yang, D. Correlations/estimation of equilibrium interfacial tension for methane/CO_2-water/brine systems based on mutual solubility. *Fluid Phase Equilib*. **2019**, 483, 197-208.

[31] Li, R.; Li, H. Improved three-phase equilibrium calculation algorithm for water/hydrocarbon mixtures. *Fuel*. **2019**, 244, 517-527.

[32] Hu, J.; Duan, Z.; Zhu, C.; Chou, I. PVTx properties of the CO_2-H_2O and CO_2-H_2O-NaCl systems below 647 K: assessment of experimental data and thermodynamic models. *Chem. Geol*. **2007**, 238, 249-267.

[33] Søreide, I.; Whitson, C. Peng-Robinson predictions for hydrocarbons, CO_2, N_2, and H_2S with pure water and NaCl brine. *Fluid Phase Equilib*. **1992**, 77, 217-240.

[34] Sørensen, H.; Pedersen, K.; Christensen, P. Modeling of gas solubility in brine. *Org. Geochem*. **2002**, 33, 635-642.

[35] Yan, Y.; Chen, C. Thermodynamic modeling of CO_2 solubility in aqueous solutions of NaCl and Na_2SO_4. *J. Supercrit. Fluids*. **2010**, 55, 623-634.

[36] Gross, J.; Sadowski, G. Perturbed-chain SAFT: an equation of state based on a perturbation theory for chain molecules. *Ind. Eng. Chem*. *Res.* **2001**, 40, 1244-1260.

[37] Song, Y.; Chen, C. Symmetric electrolyte nonrandom two-liquid activity coefficient model. *Ind. Eng. Chem*. *Res.* **2009**, 48, 7788-7797.

CHAPTER 2 METHODOLOGY

2.1 PR EOS Model

The PR EOS[1] can be expressed as:

$$p = \frac{RT}{v-b} - \frac{a}{v(v+b)+b(v-b)} \tag{1}$$

where p is the pressure in bar; v stands for molar volume in cm^3/mol; T is the temperature in K; a and b are two equation of state constants with units of $bar \cdot cm^6/mol^2$ and cm^3/mol, respectively, and they can be determined by **Equations (2)** to **(3)**:

$$a = 0.457535 \frac{R^2 T_c^2}{p_c} \alpha \tag{2}$$

$$b = 0.077796 \frac{RT_c}{p_c} \tag{3}$$

where R is the universal gas constant in $J/(mol \cdot K)$; T_c is critical temperature in K; p_c is the critical pressure in bar; and α is the so-called alpha function.

2.2 α Function

In this work, Twu α function[2] and Gasem[3] α function are used. Compared with other types of α functions, Twu α function can more accurately describe the VLE of the systems containing polar components [2,4]. The Gasem α function improves the estimates on critical properties as well as the accuracy of the VLE calculations[3,5].

The expression of Twu α function can be written as[2]:

$$\alpha(T_r) = T_r^{N(M-1)} \exp[L(1 - T_r^{MN})] \tag{4}$$

where T_r is the reduced temperature; L, M and N are compound-specific parameters. Their values are recently updated by Martinez *et al.*[4]. **Table 1** lists the values of these three parameters.

Table 1 Twu α function parameters used in this study[4].

Component	*L*	*M*	*N*
H_2O	0.3872	0.8720	1.9668
CO_2	0.1784	0.8590	2.4107

In 2001, Gasem *et al.*[3] proposed a new temperature-dependent α function which can be expressed by[3]:

$$\alpha(T) = \exp\left((A + BT_r)\left(1 - T_r^{C+D\omega+E\omega^2}\right)\right) \tag{5}$$

where the values of correlation parameters A through E are 2.0, 0.836, 0.134, 0.508 and -0.0467, respectively.

2.3 Mixing Rules

Mixing rules have a great impact on phase equilibrium calculations. In 1979, Huron and Vidal[6] proposed a new expression by considering the excess Gibbs energy for CEOS, which made more accurate the phase-composition predictions for mixtures containing polar substances. Furthermore, according to the comprehensive study by Aasen *et al.*[7], the most accurate thermodynamic model among the ones examined by them is PR EOS coupled with Twu α function and Huron-Vidal mixing rule, which provides $4.5\%AAD$ in reproducing the phase-composition data measured for CO_2/H_2O mixtures. Hence, in the first part of this study, we collect more phase equilibria data for CO_2/H_2O mixtures to verify the performance of the model suggested by Aasen *et al.*[7]. These additional experimental data are not included in the study by Aasen *et al.*[7].

Besides, based on the study by Abudour *et al.*[8], Gasem[3] α function with van der Waals (vdW) one-fluid mixing rule and their temperature-dependent volume translation function provided a

promising means to well reproduce the measured liquid-phase densities for CO_2/H_2O mixtures. Therefore, in this study, we also employ the model suggested by Abudour *et al*.[8] to test if it outperforms the model suggested by Aasen *et al*.[7].

2.3.1 Van Der Waals One-Fluid Mixing Rule

The van der Waals one-fluid mixing rule can be expressed as[9]:

$$a_m = \sum_{i=1}^{n}\sum_{j=1}^{n} z_i z_j \sqrt{a_i a_j}\left(1 - kc_{ij}\right) \tag{6}$$

$$b_m = \sum_{i=1}^{n}\sum_{j=1}^{n} z_i z_j \frac{\left(b_i + b_j\right)}{2}\left(1 + kd_{ij}\right) \tag{7}$$

where z_i is the molar fraction of the ith component in the mixture; a_i and b_i can be calculated by **Equations (2)** and **(3)**; kc_{ij} and kd_{ij} are the BIPs that need to be fitted. Abudour *et al*.[5] have regressed several linear temperature-dependent BIP correlations for CO_2/H_2O mixtures. They reported that the use of both kc_{ij} and kd_{ij} can provide more accurate estimates on both aqueous-phase and CO_2-rich-phase phase-composition predictions compared with the use of only kc_{ij}. **Table 2** lists the BIP correlations obtained by Abudour *et al*.[5].

Table 2 BIPs correlations in the van der Waals mixing rule as obtained by Abudour *et al*.[5].

Case No.	$\boldsymbol{kc_{ij} = AT + B}$		$\boldsymbol{kd_{ij} = AT + B}$	
	A	***B***	***A***	***B***
Case 2	0.00058	0.08149	0.00029	-0.31262

When the vdW mixing rule is used in PR EOS, the fugacity coefficient can be written as:

$$\ln\varphi_i = \frac{bb_i}{b_m}(Z-1) - \ln(Z-B) - \frac{A}{2\sqrt{2}B}\left(\frac{2aa_i}{a_m} - \frac{bb_i}{b_m}\right)\ln\left(\frac{Z+\left(1+\sqrt{2}\right)B}{Z-\left(1+\sqrt{2}\right)B}\right) \tag{8}$$

where:

$$bb_i = 2\sum_{j=1}^{n} z_j \frac{b_i + b_j}{2}\left(1 + kd_{ij}\right) - b_m \tag{9}$$

$$aa_i = \sum_{j=1}^{n} z_j \sqrt{a_i a_j}\left(1 - kc_{ij}\right) \tag{10}$$

where Z is the compressibility factor. For PR EOS, Z can be calculated by **Equation (11)**.

$$Z^3 - (1 - B)Z^2 + (A - 3B^2 - 2B)Z - (AB - B^2 - B^3) = 0 \tag{11}$$

where

$$A = \frac{a_m p}{R^2 T^2} \tag{12}$$

$$B = \frac{b_m p}{RT} \tag{13}$$

2.3.2 Huron-Vidal Mixing Rule

In the Huron-Vidal mixing rule, the following equations are applied to calculate a_m and b_m[6]:

$$b_m = \sum_{i=1}^{n}\sum_{j=1}^{n} z_i z_j \frac{\left(b_i + b_j\right)}{2} \tag{14}$$

$$a_m = b_m\left[\sum_{i=1}^{n} z_i \frac{a_i}{b_i} - \frac{G_\infty^E}{\Lambda}\right] \tag{15}$$

where G_∞^E is the excess Gibbs energy at infinite pressure; and Λ is an EOS-dependent parameter. For PR-EOS, $\Lambda = 0.62323$[6].

The excess Gibbs energy corresponding to the Non-Random Two-Liquid (NRTL)[10,11] model can be expressed by[6,7]:

$$G_{\infty}^{E} = RT\sum_{i=1}^{n} z_i \frac{\sum_{j=1}^{n}\tau_{ji}b_j z_j \exp\left(-\alpha_{ji}\tau_{ji}\right)}{\sum_{k=1}^{n} b_k z_k \exp(-\alpha_{ki}\tau_{ki})} \tag{16}$$

where

$$\tau_{ji} = \frac{\Delta g_{ji}}{RT} \tag{17}$$

$$g_{ii} = -\Lambda\frac{a_i}{b_i} \tag{18}$$

$$g_{ij} = -2\frac{\sqrt{b_i b_j}}{b_i + b_j}\sqrt{g_{ii}g_{jj}}\left(1 - k_{ij}\right) \tag{19}$$

The generalized BIP correlations for τ_{ij} obtained by Aasen *et al*.[7] are given below:

$$\frac{g_{12}}{RT_0} = 5.831 - 2.559\left(\frac{T}{T_0}\right) \tag{20}$$

$$\frac{g_{21}}{RT_0} = -3.311 + 0.03770\left(\frac{T}{T_0}\right) \tag{21}$$

where T_0 = 1000 K is the reference temperature.

When the Huron-Vidal mixing rule is used in PR EOS, the fugacity coefficient can be calculated by[10]:

$$\ln\varphi_i = \frac{b_i}{b_m}(Z-1) - \ln(Z-B) - \frac{1}{2\sqrt{2}}\left(\frac{a_i}{b_i RT} + \frac{\ln\gamma_i}{\Lambda}\right)\ln\left(\frac{Z+\left(1+\sqrt{2}\right)B}{Z-\left(1+\sqrt{2}\right)B}\right) \tag{22}$$

where $\ln\gamma_i$ is the activity coefficient of component *i* and can be expressed as[10]:

$$\ln\gamma_i = \frac{\sum_{j=1}^{n}\tau_{ji}z_j b_j \exp\left(-\alpha_{ji}\tau_{ji}\right)}{\sum_{k=1}^{n} z_k b_k \exp(-\alpha_{ki}\tau_{ki})} + \sum_{j=1}^{n}\left[\frac{b_i z_j \exp(-\alpha_{ij}\tau_{ij})}{\sum_{k=1}^{n} z_k b_k \exp\left(-\alpha_{kj}\tau_{kj}\right)}\cdot\left(\tau_{ij} - \frac{\sum_{l=1}^{n}\tau_{lj}z_l b_l \exp\left(-\alpha_{lj}\tau_{lj}\right)}{\sum_{k=1}^{n} z_k b_k \exp\left(-\alpha_{kj}\tau_{kj}\right)}\right)\right] \tag{23}$$

The derivation of the expression of the activity coefficient in Huron-Vidal mixing rule is detailed in **Appendix A**.

2.4 Volume Translation Models

2.4.1 Constant Volume Translation

To improve volume calculations without affecting phase equilibrium calculations, Peneloux *et al*.[12] developed a constant volume translation model in SRK EOS, while Jhaveri and Youngren[13] developed a constant volume translation model in PR EOS[1]. The constant volume translation can be expressed as[12,13]:

$$v_{corr} = v_{EOS} - \sum_{i=1}^{n} z_i c_i \tag{24}$$

where v_{corr} is corrected molar volume in cm^3/mol; v_{EOS} stands for PR-EOS-calculated molar volume in cm^3/mol; z_i is the mole fraction of the ith component in a given phase; and c_i is the component-dependent volume shift parameter which can be determined by **Equation (25)**[14].

$$c_i = s_i \times b_i \tag{25}$$

The values of s_i used by Liu *et al*.[15] are applied in this study (s_{H2O} = 0.23170 and s_{CO2} = -0.15400).

2.4.2 Volume Translation Model Developed by Abudour *et al.*[8]

In 2013, Abudour *et al*.[8] revised the temperature-dependent volume translation function to improve both saturated and single-phase liquid density calculations. Their model is given below[8]:

$$v_{corr} = v_{EOS} + c - \delta_c \left(\frac{0.35}{0.35 + d} \right) \tag{26}$$

where δ_c is volume correction at the critical temperature in cm^3/mol; and d is the dimensionless distance function given by[8]:

$$d = \frac{1}{RT_C} \left(\frac{\partial p^{PR}}{\partial \rho} \right)_T \tag{27}$$

where ρ is the molar density in mol/cm^3. The reason to introduce the distance function in the original volume translation function is to improve the accuracy of the CEOS calculated results in the near-critical region. The volume translation function proposed by Abudour *et al.*[8] was extended to mixtures by the following equations[8]:

$$v_{corr} = v_{EOS} + c_m - \delta_{c_m}\left(\frac{0.35}{0.35 + d_m}\right) \tag{28}$$

where[8]:

$$c_m = \left(\frac{RT_{c_m}}{p_{c_m}}\right)\left(c_{1_m} - \left(0.004 + c_{1_m}\right)e^{-2d_m}\right) \tag{29}$$

$$c_{1_m} = \sum_{i=1}^{n} z_i c_{1_i} \tag{30}$$

$$d_m = \frac{1}{RT_{c_m}}\left(\frac{\partial p^{PR}}{\partial \rho}\right)_T - \left(\frac{1}{RT_{c_m}\rho^2}\right)\frac{a_{v1}^2}{a_{11}} \tag{31}$$

where T_{cm}, p_{cm} and δ_{cm} are mixture's critical temperature, critical pressure and volume correction at the critical point, respectively. The second term in d_m is the molar Helmholtz energy term; it is ignored in this study since it has little effect on the volume correction[16]. c_1 has a linear relationship with critical compressibility (Z_c)[8]:

$$c_1 = 0.4266Z_c - 0.1101 \tag{32}$$

The term d_m can be derived using the original PR EOS[16]:

$$d_m = \frac{v^2}{RT_{c_m}}\left[\frac{RT}{(v-b)^2} - \frac{2a(v+b)}{(-b^2 + 2bv + v^2)^2}\right] \tag{33}$$

Mixture's volume correction δ_{cm} at the critical point of the given mixture can be determined by[8]:

$$\delta_{c_m} = 0.3074 \frac{RT_{c_m}}{p_{c_m}} - \sum_{i=1}^{n} \theta_i v_{c_i} \tag{34}$$

where v_{ci} is the critical volume of component i; θ_i is the surface fraction of component i defined by[8]:

$$\theta_i = \frac{z_i v_{c_i}^{2/3}}{\sum_{i=1}^{n} z_i v_{c_i}^{2/3}} \tag{35}$$

Mixture's critical temperature can be calculated via the following mixing rule[8].

$$T_{c_m} = \sum_{i=1}^{n} \theta_i T_{c_i} \tag{36}$$

Mixture's critical pressure can be determined by the correlation proposed by Aalto *et al.*[17]:

$$p_{c_m} = \frac{(0.2905 - 0.085\omega_m) RT_{c_m}}{\sum_{i=1}^{n} \theta_i v_{c_i}} \tag{37}$$

where ω_m is mixture's acentric factor:[8]

$$\omega_m = \sum_{i=1}^{n} z_i \omega_i \tag{38}$$

where ω_i is the acentric factor of component i.

2.5 IFT Correlations for CO_2/H_2O Mixtures

2.5.1 Parachor Model

Parachor model[18] is one of the most widely used methods in determining IFT. It can be expressed as below[19]:

$$\sigma = \left[\sum_{i=1}^{n} P_i(x_i\rho_L^M - y_i\rho_V^M)\right]^4 \quad (39)$$

where x_i and y_i are the mole fractions of component i in liquid and vapor phases, respectively; P_i is the Parachor value of component i (P_{H2O} = 52, P_{CO2} = 78)[15]; ρ_L^M is the molar density of liquid phase in mol/cm^3; and ρ_V^M is the molar density of vapor phase in mol/cm^3.

2.5.2 IFT Correlation Proposed by Chen and Yang[20]

In 2018, Chen and Yang[20] proposed a new IFT correlation for $CH_4/CO_2/H_2O$ ternary mixtures based on the mutual solubility in the equilibrating phases. As for CO_2/H_2O binaries, Chen and Yang's correlation is given as[20]:

$$\sigma = C_1 + (C_2 p_r + C_3)\ln K_{CO2} + (C_4 p_r + C_5)\ln K_{H2O} \quad (40)$$

where σ is IFT in mN/m; p_r is the reduced pressure of CO_2; C_1 to C_5 are empirical coefficients. Chen and Yang proposed four groups of coefficient set, i.e., one coefficient set (using one coefficient set on the whole pressure range) with or without the reduced pressure term, and two coefficient sets (dedicated to the pressure ranges of p≤73.8 bar and p>73.8 bar) with or without the reduced pressure term. Since using the reduced pressure term can improve prediction accuracy[20], we introduce the reduced pressure term in this study. **Table 3** lists the values of these coefficients in different coefficient set groups. Note that the density of the two equilibrating phases is not one input in Chen and Yang's correlation[20].

Table 3 Coefficients in Chen and Yang's correlation[20].

Coefficient set	Pressure range	C_1	C_2	C_3	C_4	C_5
1	Full	-63.420	2.765	15.275	2.348	-7.617
2	$p \le 73.8$ bar	-25.120	5.912	9.740	7.024	-6.857
	Else	-83.614	1.273	23.802	0.752	-4.065

To make fair comparisons, we refit these coefficients based on the IFT database employed in this study. **Table 4** summarizes the values of these refitted coefficients.

Table 4 Refitted coefficients in Chen and Yang's correlation[20].

Coefficient set	Pressure range	C_1	C_2	C_3	C_4	C_5
1	Full	-64.7356	2.3405	16.3306	2.0919	-7.1593
2	$p \leq 73.8$ bar	-34.3182	6.5500	10.8716	7.9611	-7.9076
	Else	-49.7215	0.2460	18.0648	0.1813	-1.9879

2.5.3 IFT Correlation Proposed by Hebach *et al.*[21]

In 2002, Hebach *et al*.[21] proposed a new IFT correlation for CO_2/H_2O binaries. This correlation can be expressed as[21]:

$$\sigma = k_0\left(1-\exp\left(k_1\sqrt{dd}\right)\right) + k_2\cdot dd + k_3\cdot dd^2 + k_4\cdot dd^3 + k_5\exp\left(k_6(dd - 0.9958 g^2/cm^6)\right) \tag{41}$$

where[21]:

$$dd = (\rho_{H2O} - \rho_{corr})^2 \tag{42}$$

$$\rho_{corr} = \begin{cases} \frac{\rho_{CO2} + b_0(304K - T)(10\times p)^{b_1}}{1000} & 0.025\,\mathrm{g/cm^3} < \rho_{CO2} < 0.25\,\mathrm{g/cm^3} \\ \rho_{CO2} & \text{in other cases} \end{cases} \tag{43}$$

where ρ_{CO2} is CO_2-rich-phase density in g/cm^3; ρ_{H2O} is aqueous-phase density in g/cm^3; k_0 to k_6 and b_0 to b_1 are empirical coefficients. The units of T, p, and dd are K, bar, and g^2/cm^6, respectively. **Table 5** lists the values of these coefficients. To make fair comparison, we refit these coefficients based on the IFT database employed in this study. **Table 6** summarizes the values of these refitted coefficients.

Table 5 Coefficients in Hebach *et al*. correlation[21].

Coefficients	Value
b_0 (g/(cm^3·K))	0.00022
b_1	-1.9085
k_0 (mN/m)	27.514
k_1 (cm^6/g^2)	-35.25
k_2 (cm^{12}/g^4)	31.916
k_3 (cm^{18}/g^6)	-91.016
k_4 (cm^3/g)	103.233
k_5 (mN/m)	4.513
k_6 (g^2/cm^6)	351.903

Table 6 Refitted coefficients in Hebach *et al*. correlation[21].

Coefficients	Value
b_0 (g/(cm^3·K))	0.00022
b_1	-1.9085
k_0 (mN/m)	25.6836
k_1 (cm^6/g^2)	-218.4717
k_2 (cm^{12}/g^4)	9.3192
k_3 (cm^{18}/g^6)	-0.9621
k_4 (cm^3/g)	33.4068
k_5 (mN/m)	14.4970
k_6 (g^2/cm^6)	10.9290

2.5.4 IFT Correlation Proposed in This Study

Before we finalize our IFT correlation, we implement several scenarios to find the optimal settings to represent IFT of CO_2/H_2O mixtures. Since Parachor model is one of the most widely used models in mixtures' IFT predictions, we revise the original Parachor model by introducing a component-dependent correction term α_i; furthermore, we replace the constant exponential term in the original Parachor model by correlating it with several physical properties (e.g., equilibrium ratios). The new IFT correlation can be expressed as follows:

$$\sigma = \left[\sum_{i=1}^{n} \alpha_i P_i (x_i \rho_L^M - y_i \rho_V^M)\right]^n \tag{44}$$

First, we set the component-dependent correction term α_i is a constant for each component, and the exponential term *n* can be expressed by equilibrium ratios of CO_2-rich phase and aqueous phase:

$$n = C_1 \ln K_{CO2} + C_2 \ln K_{H2O} + C_3 \quad (45)$$

Since using one coefficient set for both α_i and coefficients in **Equation (45)** cannot converge after reaching the maximum iterations, we used two coefficient sets based on CO_2-rich-phase densities. **Table 7** listed the values of these coefficients and α_i determined by fitting the proposed correlation (abbreviated as Scenario #1) to the IFT training dataset.

Table 7 Values of coefficients and α_i in Scenario #1.

Coefficients	$\rho_{CO2\text{-rich}} < 0.2$ **g/cm^3**	$\rho_{CO2\text{-rich}} \geq 0.2$ **g/cm^3**
α_{CO2}	0.7957	0.1520
α_{H2O}	0.8855	0.9509
C_1	-0.0727	0.1026
C_2	0.1044	0.0736
C_3	5.5730	3.9154

Since using constants to represent α_i leads to a larger *%AAD* compared with the refitted Chen and Yang's correlation[20] (i.e., 8.8746*%AAD* vs. 7.8520*%AAD*), we correlate equilibrium ratios to α_i to see if it can improve IFT predictions. The expression of *n* in this scenario (abbreviated as Scenario #2) is the same as that in Scenario #1. The expression for α_i is given as:

$$\alpha_i = C_1 \ln K_{CO2} + C_2 \ln K_{H2O} + C_3 \quad (46)$$

Specifically, when the CO_2-rich-phase density is greater than 0.2 g/cm^3, α_{H2O} can be simplified as:

$$\alpha_{H2O} = C_1 \ln K_{CO2} + C_3 \quad (47)$$

Table 8 listed the values of these coefficients determined by fitting the proposed correlation to the IFT training dataset.

Table 8 Values of coefficients in Scenario #2.

Coefficients	$\rho_{CO2\text{-}rich} < 0.2$ g/cm^3			$\rho_{CO2\text{-}rich} \geq 0.2$ g/cm^3		
	C_1	C_2	C_3	C_1	C_2	C_3
α_{CO2}	-0.4685	-0.2177	1.7944	0.4583	0.0107	-1.3451
α_{H2O}	-0.1033	0.0311	1.8397	0.5259	-	-0.3583
n	0.3599	-0.0855	1.3153	-0.2685	0.0124	3.5123

As shown in **Table 8**, using correlations to represent α_i can slightly improve IFT predictions (i.e., 8.3170*%AAD* in Scenario #2 vs. 8.8746*%AAD* in Scenario #1). Besides, we find that the value of n is around 4 over a wide range of temperature/pressure conditions in all scenarios (i.e., its value only slightly changes with the change of equilibrium ratios); therefore, we set the value of n as 4 for convenience.

We also find that using two coefficient sets based on CO_2-rich-phase density range in our correlation leads to inconsistent IFT predictions. In addition, based on the study by Chen and Yang[20], introducing CO_2's reduced pressure can improve IFT predictions. Thus, we introduce CO_2's reduced pressure in the expressions of α_i and use one coefficient on the whole CO_2-rich-phase density range to see if these settings can further improve prediction accuracies without yielding inconsistent IFT predictions.

Based on the calculation results, the aforementioned settings of IFT correlation yield the lowest *%AAD* among others examined in this study. The new IFT correlation is finalized as:

$$\sigma = \left[\sum_{i=1}^{n} \alpha_i P_i (x_i \rho_L^M - y_i \rho_V^M)\right]^4 \tag{48}$$

where the α_i term in the new correlation can be expressed as:

$$\alpha = C_1 + (C_2 p_r + C_3)\ln K_{CO2} + (C_4 p_r + C_5)\ln K_{H2O} \quad (49)$$

Table 9 lists the values of these coefficients determined by fitting the proposed correlation to the IFT training dataset.

Table 9 Coefficients in the α_i term for H_2O and CO_2.

Component	C_1	C_2	C_3	C_4	C_5
H_2O	1.1325	-0.0085	-0.0083	0.0134	0.0089
CO_2	-0.4193	-0.0057	-0.0320	0.0209	-0.1430

We also implement deep neural network (DNN) and convolutional neural network (CNN) to model the IFT of CO_2/H_2O mixtures. The inputs of these models are equilibrium ratios, temperature, pressure, phase compositions, and phase densities. Although these models yield relatively lower *%AAD*s compared with the newly proposed empirical IFT correlation, neural network models bear inconsistent issues partially due to the lack of enough training data points. Thus, we only apply the newly proposed empirical correlation to calculate IFT of CO_2/H_2O mixtures in this study.

2.6 Data Selection and Evaluation

2.6.1 Phase Equilibrium Data

Table 10 summarizes the measured phase equilibrium data of CO_2/H_2O mixtures over 278-378.15 K and 6.9-709.3 bar reported in the literature[22-31]. Note that these experimental data were not included in the study by Aasen *et al*.[7].

Table 10 Phase equilibrium data of CO_2/H_2O mixtures employed in this study.

T (K)	P (bar)	x_{CO2}(%)[a]	y_{H2O}(%)[b]	NDP[c]	References
323.15-373.15	25.3-709.3	0.429-3.002	-	29[d]	22
285.15-313.15	25.3-506.6	0.925-3.196	-	42[e]	23
323.15-373.15	200-500	2-2.8	1-3	4[f]	24
288.71-366.45	6.9-202.7	0.0973-2.63	0.0819-12.03	24[g]	25
323.15	68.2-176.8	1.651-2.262	0.339-0.643	8	26
285.15-304.21	6.9-103.4	-	0.0603-0.33739	9[h]	27
323.15-348.15	101.33-152	1.56-2.1	0.55-0.9	4	28
348.15	103.4-209.4	1.91-1.92	0.63-0.84	2/3[i]	29
323.15	101-301	2.075-2.514	0.547-0.782	3	30
278-293	64.4-294.9	2.5-3.49	-	24	31

a: Solubility of CO_2 in the aqueous phase
b: Solubility of H_2O in the CO_2-rich phase
c: Number of data points
d, e, f, g, h, and i: these data are already summarized by Spycher *et al*.[32] We directly use these data mentioned in their paper for convenience.
i: NDP for x_{CO2} is 2 and NDP for y_{H2O} is 3.

2.6.2 Phase Density Data

Table 11 summarizes the experimental aqueous-phase and CO_2-rich-phase density data of CO_2/H_2O mixtures over 278-478.35 K and 2.5-1291.1 bar documented in the literature. **Figure 1** shows the pressure-temperature coverage of the phase density data collected from the literature[31, 33-42].

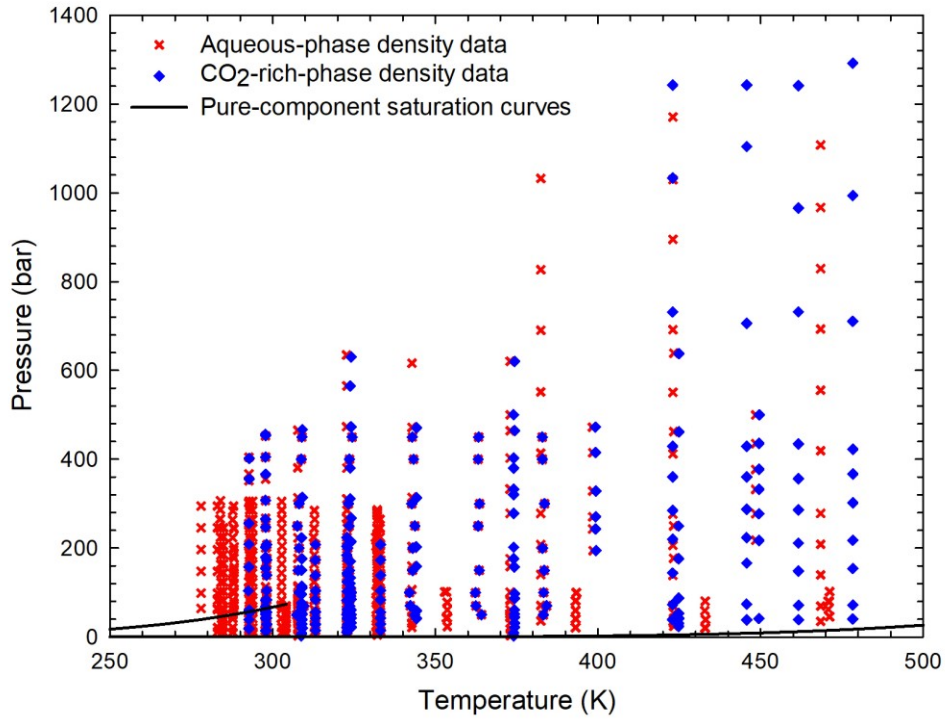

Figure 1 Pressure-temperature coverage of the phase-density data collected from the literature. The solid curves stand for pure-CO_2 (left) and pure-H_2O (right) saturation curves, respectively.

Table 11 Aqueous-phase (ρ_{H2O}) and CO_2-rich-phase ($\rho_{CO2\text{-}rich}$) density data of CO_2/H_2O mixtures employed in this study.

***T* (K)**	***P* (bar)**	**ρ_{H2O} (kg/m^3)**	**$\rho_{CO2\text{-}rich}$ (kg/m^3)**	**NDP**	**References**
288.15-298.15	60.8-243.2	1015-1027	-	27	33
278-293	64.4-294.9	1013.68-1025.33	-	24	31
352.85-471.25	21.1-102.1	840-963	-	33	34
304.1	10-70	999.4-1011.8	18.8-254.2	8	35
332.15	33.4-285.9	990.5-1010.3	-	29	36
283.8-333.19	10.8-306.6	983.7-1031.77	-	200	37
307.4-384.2	50-450	950.6-1026.1	80.8-987.5	42	38
322.8-322.9	11-224.5	988.52-1009.13	18.8484-812.725	11	39
382.41-478.35	34.82-1291.9	871.535-994.984	36.943-944.965	30/40[a]	40
298.15-333.15	14.8-207.9	984.6-1022	24.6-907.1	36	41
292.7-449.6	2.5-638.9	905.9-1034.9	4.6-1023.4	144/128[b]	42

a: NDP for ρ_{H2O} is 30 and NDP for $\rho_{CO2\text{-}rich}$ is 40.
b: NDP for ρ_{H2O} is 144 and NDP for $\rho_{CO2\text{-}rich}$ is 128.

2.6.3 IFT Data

Table 12 summarizes the experimental IFT data for CO_2/H_2O mixtures over 278.15-477.59 K and 1-1200.96 bar documented in the literature[15,21,38-39,43-54]. Ideally, phase densities should be directly measured; however, only Chiquet *et al*.[38], Kvamme *et al*.[39], Bikkina *et al*.[41], Bachu and Bennion[49], and Shariat *et al*.[52] applied measured phase densities in IFT calculations. In order to expand our IFT database, IFT data with precisely determined phase densities are also included in our IFT database. **Figure 2** shows the pressure-temperature coverage of the IFT data of CO_2/H_2O mixtures collected from the literature with 589 data points in the training dataset and 189 data points in the validation dataset.

Table 12 Measured IFT data for CO_2/H_2O mixtures used in this study.

T **(K)**	***P*** **(bar)**	**IFT (mN/m)**	**NDP**	**References**
311-411	1-689.48	17.40-58.40	58	43
311.15-344.15	1-197.8	17.63-69.20	28	44
278.15-344.15	1-186.1	18.27-74.27	114[a]	45
311.15-344.15	1.6-310.7	19.38-56.86	20	46
278.4-333.3	1-200.3	12.4-74	85	21
293.15-344.15	1-202.8	20.55-78.01	26[b]	47
318.15	11.6-165.6	25.4-70.5	14	48
322.8-322.9	11-224.5	29.1-63.7	11	39
307.4-384.2	50-450	45.8-22.8	43	38
293.15-398.15	20-270	18.9-68.1	87[c]	49
344.15	28.57-245.24	25.49-45.01	11	50
297.8-374.3	10-600.5	21.23-65.73	80	51
298.15-333.15	14.8-207.9	22.16-59.66	36	41
323.15-477.59	77.78-1200.96	10.37-35.38	21	52
284.15-312.15	10-60	29.02-66.98	30	53
298.4-469.4	3.4-691.4	12.65-68.52	78	54
299.8-398.15	7.86-344.12	28.04-68.23	36	15

a, b, and c: Some experimental data appear to be outliers and hence excluded for further analysis due to the significant deviation from other experimental data at similar temperature and pressure conditions (See **Figures 3** and **4**).

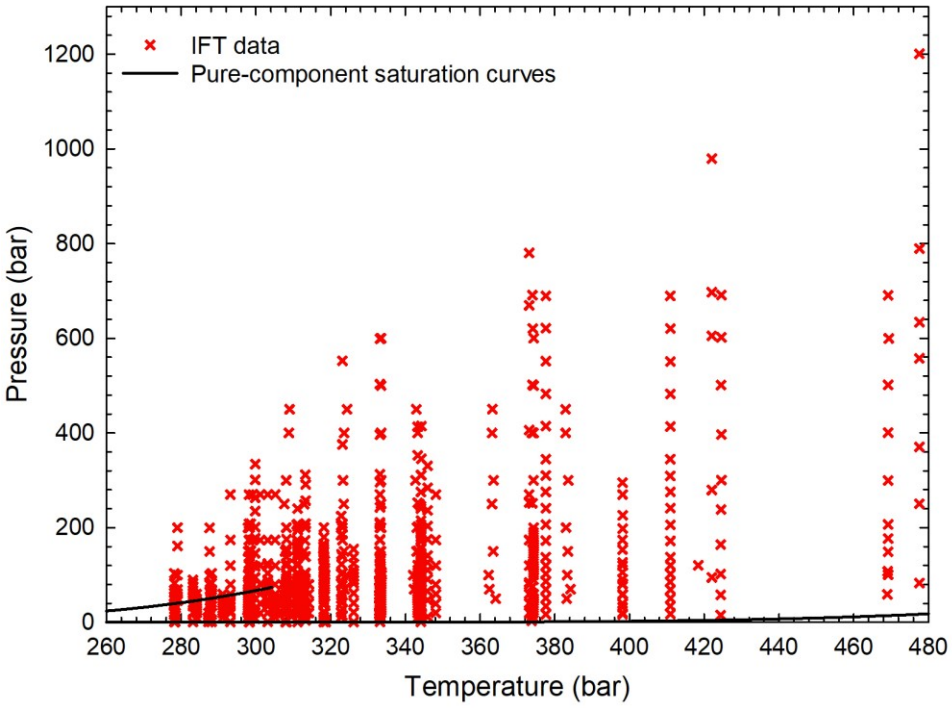

Figure 2 Pressure-temperature coverage of the IFT data for CO_2/H_2O mixtures collected from the literature.

The collected IFT data are further screened to remove any obvious outliers. **Figure 3** shows the identification of the outliers from the collected data over 40-60 bar and 278.15-298.15 K, while **Figure 4** shows the identification of outliers from the collected data over 100-270 bar and 307.15-314.15 K.

As seen in **Figure 3a**, the measured IFT data by Chun and Wilkinson[45] and Park *et al*.[47] fall into the range of 5-8 mN/m over 278.15-288.15 K and 40-60 bar, which are significantly lower than the measured IFT data (i.e., around 22-28 mN/m) obtained by other studies under similar conditions. **Figure 3b** indicates that the measured IFT data by Chun and Wilkinson[45] and Park *et al*.[47] fall into the range of 10-14 mN/m over 293.15-298.15 K and 50-70 bar, which are significantly lower than the measured IFT data (i.e., around 28-31 mN/m) obtained by other studies under similar conditions.

Figure 4 indicates that the measured data by Bachu and Bennion[49] fall into the range of 16-19 mN/m over 307.15-314.15 K and 120-270 bar, which are significantly lower than the measured IFT values (i.e., around 30 mN/m) obtained by other studies under similar conditions. No outlier exists at other temperature and pressure conditions. We have removed these outliers in the subsequent analysis.

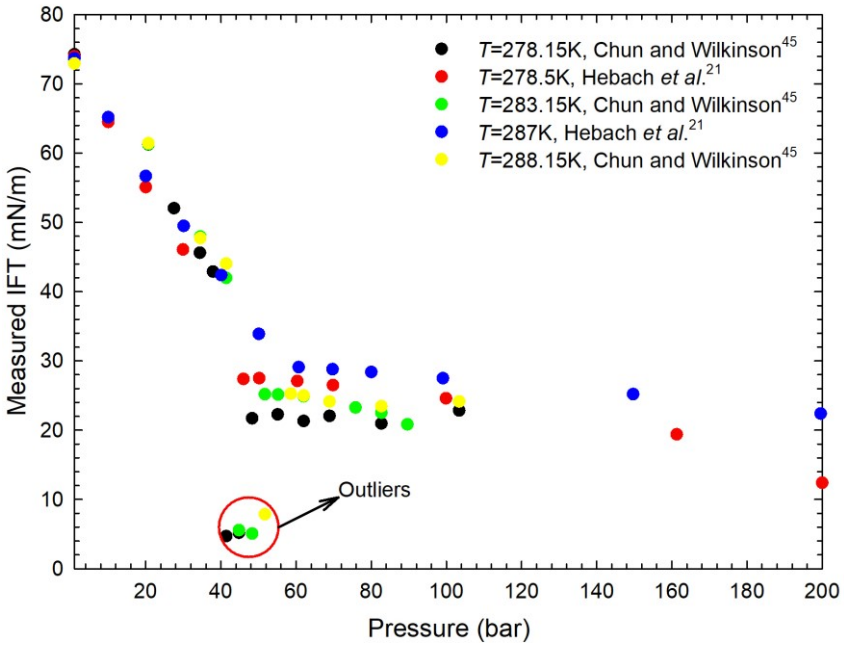

(a)

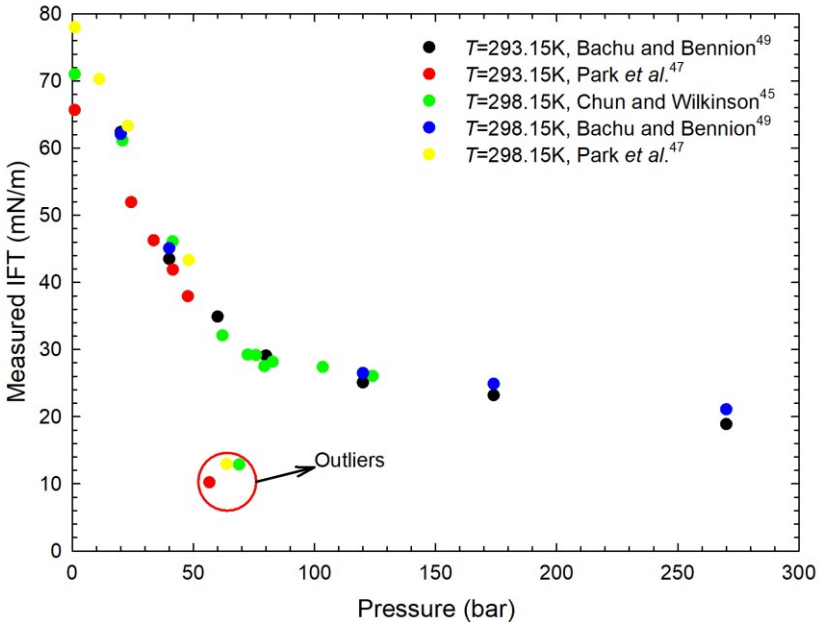

(b)

Figure 3 Identification of the outliers at T = 278.15-288.15 K (a) and T = 293.15-298.15 K (b). Outliers are from the studies by Chun and Wilkinson[45] and Park *et al*.[47].

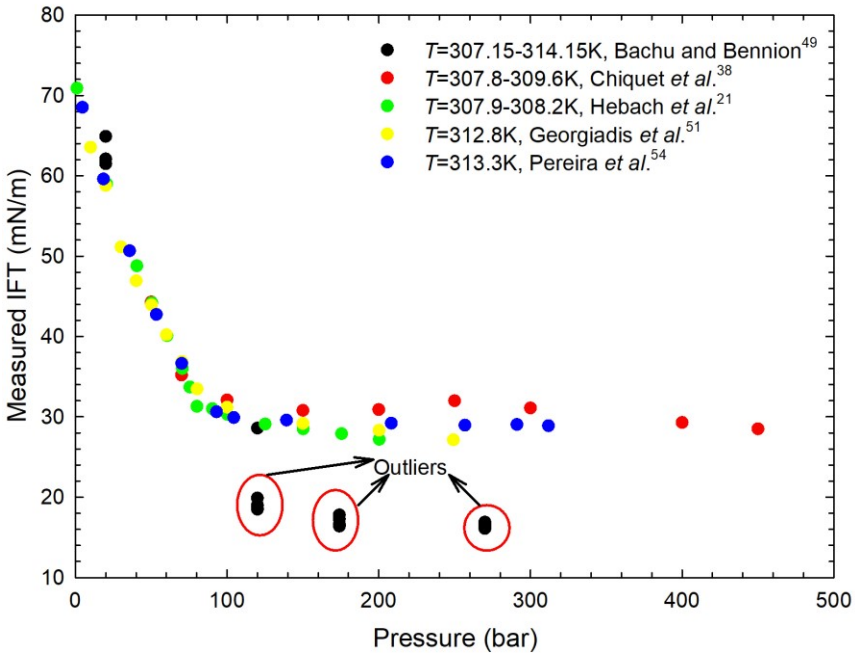

Figure 4 Identification of the outliers at moderate temperature (307.15-314.15K) conditions. Outliers are from the study by Bachu and Bennion[49].

2.7 Non-Linear Regression Algorithm

In Section 2.5, we refit both Chen and Yang[20] and Hebach *et al.*[21] IFT correlations and regress coefficients in the new IFT correlation proposed in this study. Compared with gradient descent and Gauss-Newton methods, Levenberg-Marquardt (LM) method yields more robust and faster convergence[55]. Thus, we employ LM algorithm for the non-linear regression in this study; more details about the LM algorithm can be found in the study by Madsen *et al.*[55]

2.8 Two-Phase Flash Calculations

An in-house MATLAB code is implemented in this study for the two-phase flash calculations. As denoted by Whitson and Brulé[56], the chemical potential of one phase equals that of the other phase when the two phase reaches equilibrium. Fugacity coefficient is a common expression to represent the chemical potential of each phase. When phase equilibrium exists, the following expression is used to describe such a phenomenon[56]:

$$f_{Li} = f_{Vi}, i = 1, \dots, N \tag{50}$$

where f_{Li} and f_{Vi} are the fugacity coefficients of the ith component in liquid phase and gas-rich phase, respectively.

One of the key steps in two-phase flash calculation is solving the Rachford-Rice equation[57]:

$$h(F_v) = \sum_{i=1}^{n} \frac{z_i(K_i - 1)}{1 + F_v(K_i - 1)} = 0 \tag{51}$$

where F_v is the vapor mole fraction; K_i is the so-called K-value (equilibrium ratio) and can be written as:

$$K_i = \frac{y_i}{x_i} \tag{52}$$

In this study, we implement stability test before conducting the two-phase flash calculations. The results from the stability test are used for the initialization of the K-values in two-phase flash calculations. The details of stability test can be found in the studies by Whitson and Brulé[56] and Michelsen[58].

K-values (K_i) should be initialized before the stability test by applying the following equation proposed by Wilson[59]:

$$K_i = \frac{\exp[5.37(1 + \omega_i)(1 - T_{ri}^{-1})]}{p_{ri}} \tag{53}$$

where T_{ri} and p_{ri} are the reduced temperature and reduced pressure of the ith component, respectively. The Newton-Raphson algorithm is implemented in the two-phase flash calculations to solve for F_v. Whitson and Brulé[56] provided a detailed coverage on the calculation procedures of the two-phase flash calculation algorithm in their monograph.

References

[1] Peng, D. Y.; Robinson, D. B. A new two-constant equation of state. *Ind. Eng. Chem. Fundamen.* **1976**, 15, 59-64.

[2] Twu, C. H.; Bluck, D.; Cunningham, J. R.; Coon, J. E. A cubic equation of state with a new alpha function and a new mixing rule. *Fluid Phase Equilib*. **1991**, 69, 33-50.

[3] Gasem, K.A.M.; Gao, W.; Pan, Z.; Robinson, R.L. A modified temperature dependence for the Peng-Robinson equation of state. *Fluid Phase Equilib*. **2001**, 181, 113-125.

[4] Martinez, A.; Guennec, Y.L.; Privat, R.; Jaubert, J.N.; Mathias, P.M. Analysis of the combinations of property data that are suitable for a safe estimation of consistent Twu α-Function parameters: updated parameter values for the translated-consistent tc-PR and tc-RK cubic equations of state. *J. Chem. Eng. Data*. **2018**, 63, 3980-3988.

[5] Abudour, A.M.; Mohammad, S.A.; Gasem, K.A.M. Modeling high-pressure phase equilibria of coalbed gases/water mixtures with the Peng-Robinson equation of state. *Fluid Phase Equilib*. **2012**, 319, 77-89.

[6] Huron, M.J.; Vidal, J. New mixing rules in simple equations of state for representing vapor-liquid equilibria of strongly non-ideal mixtures. *Fluid Phase Equilib*. **1979**, 3, 255-271.

[7] Aasen, A.; Hammer, M.; Skaugen, G.; Jakobsen, J.P.; Wilhelmsen, Ø. Thermodynamic models to accurately describe the PVTxy-behavior of water/carbon dioxide mixtures. *Fluid Phase Equilib*. **2017**, 442, 125-139.

[8] Abudour, A.M.; Mohammad, S.A.; Robinson R.L.; Gasen, K.A.M. Volume-translated Peng-Robinson equation of state for liquid densities of diverse binary mixtures. *Fluid Phase Equilib*. **2013**, 349, 37-55.

[9] van der Waals, J.D. Continuity of the gaseous and liquid state of matter. 1873.

[10] Zhao, H.; Lovo, S.N. Phase behavior of the CO_2-H_2O system at temperatures of 273-623 K and pressures of 0.1-200 MPa using Peng-Robinson-Stryjek-Vera equation of state with a modified Wong-Sandler mixing rule: an extension to the CO_2-CH_4-H_2O system. *Fluid Phase Equilib*. **2016**, 417, 96-10.

[11] Wong, D.S.H; Sandler, S.I. A theoretically correct mixing rule for cubic equations of state. *AIChE J*. **1992**, 38, 671-680.

[12] Peneloux, A.; Rauzy, E.; Freze, R. A consistent correction for Redlich-Kwong-Soave volumes. *Fluid Phase Equilib*. **1982**, 8, 7-23.

[13] Jhaveri, B.S.; Youngren, G.K. Three-parameter modification of the Peng-Robinson equation of state to improve volumetric predictions. *SPE Res. Eng*. **1988**, 8, 1033-1040.

[14] Young, A.F.; Pessoa, F.L.P.; Ahón, V.R.R. Comparison of volume translation and co-volume functions applied in the Peng-Robinson EOS for volumetric corrections. *Fluid Phase Equilib*. **2017**, 435, 73-87.

[15] Liu, Y.; Li, H.; Okuno, R. Measurements and modeling of interfacial tension for CO_2/CH_4/brine systems under reservoir conditions. *Ind. Eng. Chem. Res*. **2016**, 55, 12358-12375.

[16] Matheis, J.; Müller, H.; Pfitzner, M.; Hickel, S. Modeling of real fluid effects. Sonderforschungsbereich/ Transregio 40 Annual Report. 2014.

[17] Aalto, M.; Keskinen, K.I.; Aittamaa, J.; Liukkonen, S. An improved correlation for compressed liquid densities of hydrocarbons. Part 2. Mixtures. *Fluid Phase Equilib*. **1996**, 114, 21-35.

[18] Sugden, S. The Parachors and valency. 1930.

[19] Schechter, D.S.; Guo, B. Parachors based on modern physics and their uses in IFT prediction of reservoir fluids. *SPE Res. Eval. Eng*. **1998**, 1, 207-217.

[20] Chen, Z.; Yang, D. Correlations/estimation of equilibrium interfacial tension for methane/CO_2-water/brine systems based on mutual solubility. *Fluid Phase Equilib*. **2019**, 483, 197-208.

[21] Hebach, A.; Oberhof, A.; Dahmen, N.; Kögel, A.; Ederer, H.; Dinjus, E. Interfacial tension at elevated pressures – measurements and correlations in the water + carbon dioxide system. *J. Chem. Eng. Data*. **2002**, 47, 1540-1546.

[22] Weibe, R.; Gaddy, V.L. The solubility in water of carbon dioxide at 50, 75, and 100^o, at pressures to 700 atmospheres. *J. Am. Chem. Soc*. **1939**, 61, 315-318.

[23] Weibe, R.; Gaddy, V.L. The solubility of carbon dioxide in water at various temperatures from 12 to 40^o and at pressures to 500 atmospheres: critical phenomena. *J. Am. Chem. Soc.* **1940**, 62, 815-817.

[24] Tödheide, K.; Frank, E.U. Das Zweiphasengebiet und die kritische Kurve im system kohlendioxid-wasser bis zu drucken von 3500 bar. *Z. Phys. Chemie*. **1962**, 37, 387-401.

[25] Gillepsie, P.C.; Wilson, G.M. Vapor-liquid and liquid-liquid equilibria: water-methane, water-carbon dioxide, water-hydrogen sulfide, water-n-pentane, water-methane-n-pentane. Research report RR-48, Gas Processors Association, Tulsa Okla., April 1982.

[26] Briones, J.A.; Mullins, J.C.; Thies, M.C.; Kim, B.U. Ternary phase equilibria for acetic acid-water mixtures with supercritical carbon dioxide. *Fluid Phase Equilib*. **1987**, 36, 235-246.

[27] Song, K.Y.; Kobayashi, R. Water content of CO_2 in equilibrium with liquid water and/or hydrates. *SPE Form. Eval*. **1987**, 2, 500-508.

[28] D'Souza, R.; Patrick, J.R.; Teja, A.S. High pressure phase equilibria in the carbon dioxide – n-hexadecane and carbon dioxide-water systems. *Can. J. Chem. Eng*. **1988**, 66, 319-323.

[29] Sako, T.; Sugata, T.; Nakazawa, N.; Obuko, T.; Sato, M.; Taguchi, T.; Hiaki, T. Phase equilibrium study of extraction and concentration of furfural produced in reactor using supercritical carbon dioxide. *J. Chem. Eng. Jpn*. **1991**, 24, 449-454.

[30] Dohrn, R.; Bünz, A.P.; Devlieghere, F.; Thelen, D. Experimental measurements of phase equilibria for ternary and quaternary systems of glucose, water, CO_2 and ethanol with a novel apparatus. *Fluid Phase Equilib*. **1993**, 83, 149-158.

[31] Teng, H.; Yamasaki, A.; Chun, M.K.; Lee, H. Solubility of liquid CO_2 in water at temperatures from 278 K to 293 K and pressures from 6.44 MPa to 29.49 MPa and densities of the corresponding aqueous solutions. *J. Chem. Thermodyn*. **1997**, 29, 1301-1310.

[32] Spycher, N.; Pruess, K.; King, J.E. CO_2-H_2O mixtures in the geological sequestration of CO_2. I. Assessment and calculation of mutual solubilities from 12 to 100ºC and up to 600 bar. *Geochim. Cosmochim. Ac*. **2003**, 67, 3015-3031.

[33] King, M.B.; Mubarak, A.; Kim, J.D.; Bott, T.R. The mutual solubilities of water with supercritical and liquid carbon-dioxide. *J. Supercri. Fluids*. **1992**, 5, 296-302.

[34] Nighswander, J.A.; Kalogerakis, N.; Mehrotra, A.K. Solubilities of carbon dioxide in water and 1 wt% NaCl solution at pressures up to 10 MPa and temperatures from 80 to 200ºC. *J. Chem. Eng. Data*. **1989**, 34, 355-360.

[35] Yaginuma. R.; Sato. Y.; Kodama, D.; Tanaka, H.; Kato, M. Saturated densities of carbon dioxide + water mixture at 304.1 K and pressures to 10 MPa. *J. Jpn. Instit. Energy*. **2000**, 79, 144-146.

[36] Li, Z.; Dong, M.; Li, S.; Dai, L. Densities and solubilities for binary systems of carbon dioxide plus water and carbon dioxide plus brine at 59ºC and pressures to 29 MPa. *J. Chem. Eng. Data*. **2004**, 49, 1026-1031.

[37] Hebach, A.; Oberhof, A.; Dahmen, N. Density of water plus carbon dioxide at elevated pressures: measurements and correlation. *J. Chem. Eng. Data*. **2004**, 49, 950-953.

[38] Chiquet, P.; Daridon, J.; Broseta, D.; Thibeau, S. CO_2/water interfacial tensions under pressure and temperature conditions of CO_2 geological storage. *Energy Convers. Manag*. **2007**, 48, 736-744.

[39] Kvamme, B.; Kuznetsova, T.; Hebach, A.; Oberhof, A.; Lunde, E. Measurements and modelling of interfacial tension for water + carbon dioxide systems at elevated pressures. *Comput. Mater. Sci*. **2007**, 38, 506-513.

[40] Tabasinejad, F.; Barzin, Y.; Moore, G.R.; Mehta, S.A.; Fraassen, K.C.V.; Rushing, J.A.; Newsham, K.E. Water/CO_2 system at high pressure and temperature conditions:

measurement and modeling of density in equilibrium liquid and vapor phases. Paper SPE 131636 presented at the SPE EUROPEC/EAGD Annual Conference and Exhibition. Barcelona, Spain, June 14-17, 2010.

[41] Bikkina, P.K.; Shoham, O.; Uppaluri, R. Equilibrated interfacial tension data of the CO_2-water system at high pressures and moderate temperatures. *J. Chem. Eng. Data*. **2011**, 56, 3725-3733.

[42] Efika, E.C.; Hoballah, R.; Li, X.; May, E.F.; Nania, M.; Vicente, Y.S., Trusler, J.P.M. Saturated phase densities of (CO_2 + H_2O) at temperatures from (293 to 450) K and pressures up to 64 MPa. *J. Chem. Thermodyn*. **2016**, 93, 347-359.

[43] Heuer, G.J. Interfacial tension of water against hydrocarbons and other gases and adsorption of methane on solids at reservoir temperatures and pressures. PhD Dissertation, Univ. of Texas at Austin, Austin, Texas. 1957.

[44] Hough, E.W.; Henuer, G.J.; Walker, J.W. An improved pendant drop, interfacial tension apparatus and data for carbon dioxide and water. *Pet. Trans. AIME.* **1969**, 216, 469-472.

[45] Chun, B.S.; Wilkinson, G.T. Interfacial tension in high-pressure carbon dioxide mixtures. *Ind. Eng. Chem. Res*. **1995**, 34, 4371-4377.

[46] Da Rocha, S.R.P.; Harrison, K.L.; Johnston, K.P. Effect of surfactants on the interfacial tension and emulsion formation between water and carbon dioxide. *Langmuir*. **1999**, 15, 419-428.

[47] Park, J.Y.; Lim, J.S.; Yoon, C.H.; Lee, C.H.; Park, K.P. Effect of a fluorinated sodium bis (2-ethylhexyl) sulfosuccinate (aerosol-OT, AOT) analogue surfactant on the interfacial tension

of CO_2 + water and CO_2 + Ni-Plating solution in near- and supercritical CO_2. *J. Chem. Eng. Data*. **2005**, 50, 299-308.

[48] Akutsu, T.; Yamaji. Y.; Yamaguchi, H.; Watanabe, M.; Smith, R.; Inomata, H. Interfacial tension between water and high pressure CO_2 in the presence of hydrocarbon surfactants. *Fluid Phase Equilib*. **2007**, 257, 163-168.

[49] Bachu, S.; Bennion, D.B. Interfacial tension between CO_2, freshwater, and brine in the range of pressure from (2 to 27) MPa, temperature from (20 to 125) ^{o}C, and water salinity from (0 to 334000) mg • L^{-1}. *J. Chem. Eng. Data*. **2009**, 54, 765-775.

[50] Chalbaud, C.; Robin, M.; Lombard, J.M.; Martin, F.; Egermann, P.; Bertin, H. Interfacial tension measurements and wettability evaluation for geological CO_2 storage. *Adv. Water Resour*. **2009**, 32, 98-109.

[51] Georgiadis, A.; Maitland, G.; Trusler, J.P.; Bismarck, A. Interfacial tension measurements of the (H_2O + CO_2) system at elevated pressures and temperatures. *J. Chem. Eng. Data*. **2010**, 55, 4168-4175.

[52] Shariat, A.; Moore, R.G.; Mehta, S.A.; Fraassen, K.C.; Newsham, K.E.; Rushing, J.A. Laboratory measurements of CO_2-H_2O interfacial tension at HP/HT conditions: implications for CO_2 sequestration in deep aquifers. Paper CMTC 150010 presented at Carbon Management Technology Conference. Orlando, Florida, USA, February 7-9, 2012.

[53] Khosharay, S.; Varaminian, F. Experimental and modeling investigation on surface tension and surface properties of (CH_4 + H_2O), (C_2H_6 + H_2O), (CO_2 + H_2O) and (C_3H_8 + H_2O) from 284.15K to 312.15K and pressures up to 60bar. *Int. J. Refrig*. **2014**, 47, 26-35.

[54] Pereira, L.; Chapoy, A.; Burgass, R., Oliveira, M.B.; Coutinho, J.; Tohidi, B. Study of the impact of high temperatures and pressures on the equilibrium densities and interfacial tension of the carbon dioxide/water system. *J. Chem. Thermodyn*. **2016**, 93, 404-415.

[55] Madsen, K.; Nielsen, H.B.; Tingleff, O. Methods for non-linear least squares problems, 2nd edition. Informatics and Mathematical Modelling, Technical University of Denmark, April, 2004.

[56] Whitson, C.H.; Brulé, M.R. Phase behavior (vol. 20). Richardson, TX: Henry L. Doherty Memorial Fund of AIME. *SPE*. 2000.

[57] Rachford Jr, H.H.; Rice, J.D. Procedure for use of electronic digital computers in calculating flash vaporization hydrocarbon equilibrium. *J. Pet. Technol*. **1952**, 410, 19-3.

[58] Michelsen, M.L. The isothermal flash problem. Part I. Stability. *Fluid Phase Equilib.* **1982**, 9, 1-19.

[59] Wilson, G.M.A modified Redlich-Kwong equation of state, application to general physical data calculations. Paper 15c presented at the AIChE Natl. Meeting. Cleveland, Ohio, USA, 1969.

CHAPTER 3 RESULTS AND DISCUSSION

The values of critical pressure (p_c), critical temperature (T_c), acentric factor (ω), molecular weight (MW), critical compressibility factor (Z_c) used in this study are retrieved from the NIST database[1] and listed in **Table 13**.

Table 13 Pure component properties[1].

Component	p_c (bar)	T_c (K)	ω	MW	Z_c
H_2O	220.64	647.14	0.3443	18.0153	0.2294
CO_2	73.773	304.13	0.22394	44.0095	0.2746

3.1 Performance Comparison of Thermodynamic Models in Phase Equilibrium Calculations

Table 14 details the settings of four thermodynamic models examined in this work. **Table 13** summarizes the performance of different thermodynamic models in phase-composition predictions. Comparison between the measured and calculated phase-composition results is evaluated by the average absolute percentage deviation ($\%AAD$) defined as:

$$\%AAD = \frac{100}{NDP}\sum_{i=1}^{NDP}\left|\frac{x_{CAL}-x_{EXP}}{x_{EXP}}\right|_i \tag{54}$$

where x_{CAL} and x_{EXP} are the calculated and measured mole fraction of CO_2 or H_2O in the aqueous phase (or the CO_2-rich phase), respectively.

Table 14 Settings of four thermodynamic models examined in this work.

Case No.	α function	Mixing rule	BIPs
Case 1	Gasem[2]	vdW[4]	kc_{ij}=0; kd_{ij}=0
Case 2	Gasem[2]	vdW[4]	$kc_{ij}(T)$; $kd_{ij}(T)$[6]
Case 3	Twu[3]	Huron-Vidal[5]	Aasen *et al.*[7]
Case 4	Gasem[2]	Huron-Vidal[5]	Aasen *et al.*[7]

Table 15 *%AAD* of calculated CO_2's mole fraction in the aqueous phase (x_{CO2}) and H_2O's mole fraction in the CO_2-rich phase (y_{H2O}) by different thermodynamic models.

Case No.	*%AAD* for x_{CO2}	*%AAD* for y_{H2O}	Overall *%AAD*
Case 1	74.74	115.86	86.34
Case 2	6.75	16.90	9.61
Case 3	5.01	10.37	6.52
Case 4	3.22	16.59	6.99

As shown in **Table 15**, Case 4 (Gasem + HV) yields the most accurate x_{CO2} predictions among others, while Case 3 (Twu + HV) significantly outperforms other models in y_{H2O} predictions. Given the overall performance (i.e., the overall *%AAD* obtained by different models), Case 3 (Twu + HV) is found to be the optimal model in phase-composition predictions with an overall 6.52*%AAD*. **Figures 5** and **6** compares the performance of different models at T=323.15 K and T=348.15 K. As can be seen from these two figures, the thermodynamic model Case 3 (Twu + HV) can well capture the trend exhibited by the measured solubility data over a wide pressure range.

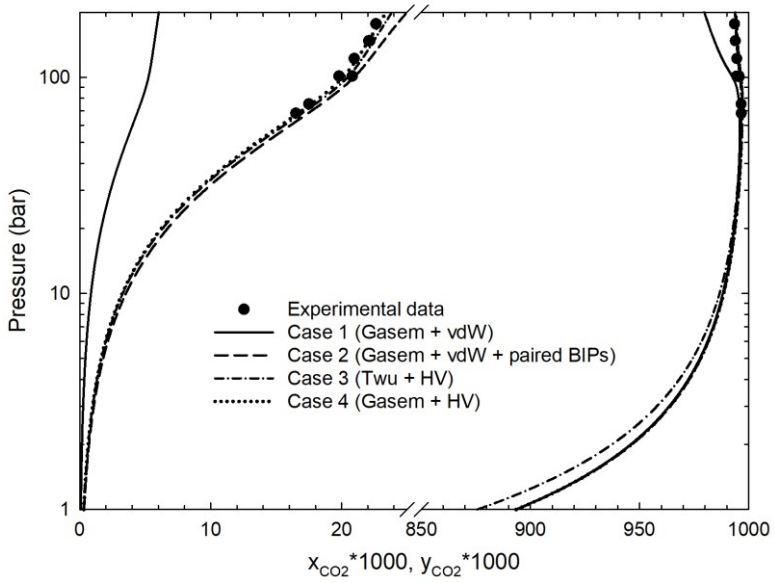

Figure 5 Measured and calculated pressure-composition data for CO_2/H_2O mixtures at T=323.15 K. Solid circles are the experimental data from the study by Briones *et al.*[8].

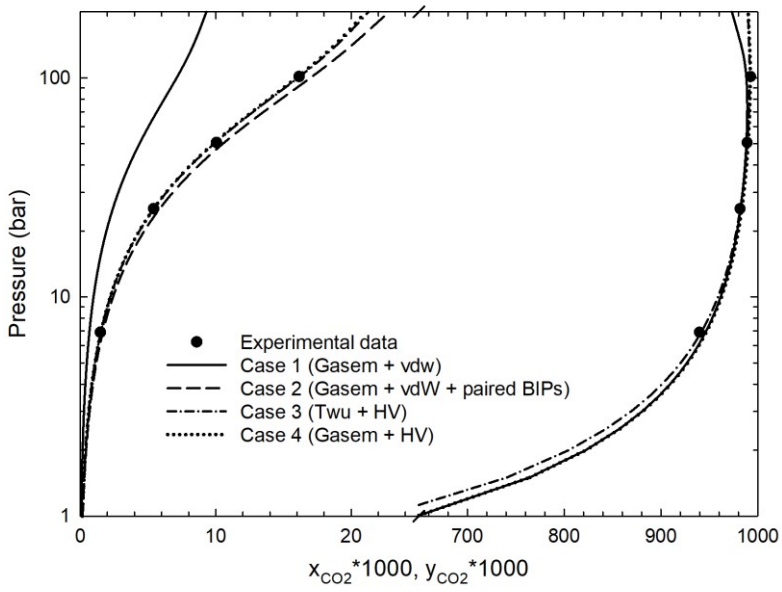

Figure 6 Measured and calculated pressure-composition data for CO_2/H_2O mixtures at T=348.15 K. Solid circles are the experimental data from the study by Gillepsie and Wilson[9].

3.2 Density-Prediction Performance of Thermodynamic Models

Since Cases 3 (Twu + HV) outperforms other thermodynamic models in phase-composition predictions for CO_2/H_2O mixtures, we only focus on the performance of Case 3 coupled with volume translation in phase-density predictions. **Table 16** summarizes the performance of different volume translation models in both aqueous-phase and CO_2-rich phase-density predictions.

Table 16 *%AAD* of the calculated aqueous-phase density (ρ_{H2O}) and CO_2-rich-phase density ($\rho_{CO2\text{-}rich}$) by different thermodynamic models.

Model	*%AAD* for ρ_{H2O}	*%AAD* for $\rho_{CO2\text{-}rich}$	Average *%AAD*
Case 3-1 Twu+ HV + Abudour *et al.*[10] VT	3.04	2.54	2.88
Case 3-2 Twu + HV + Constant VT	4.49	7.86	5.51
Case 3 (Base case) Twu +HV	15.08	3.36	11.42

As shown in **Table 16**, incorporation of VT into the thermodynamic framework can generally improve the phase-density prediction accuracy. Case 3-1 (Twu + HV + Abudour *et al.*[10] VT)

provides the most accurate estimates of both aqueous-phase and CO_2-rich-phase density, yielding 2.88*%AAD* in reproducing the measured phase-density data. **Figures 7-9** further visualize some of the calculation results by these three different models at different pressure/temperature conditions.

It can be seen from **Figures 7-9** that, regarding the aqueous-phase density predictions, the performance of Case 3-2 (Twu + HV + Constant VT) improves dramatically as temperature rises. As shown in **Figure 9**, at high temperature conditions, Case 3-2 with constant VT yields the most accurate aqueous-phase density predictions; however, it fails to accurately predict CO_2-rich phase densities. As a lighter phase, CO_2-rich phase density can be accurately predicted without the use of volume translation functions. Applying Abudour *et al*.[10] VT method is able to only slightly improve the prediction accuracy (i.e., 2.54*%AAD*). In contrast, applying constant VT in CO_2-rich-phase density predictions can lead to larger errors than the case without the use of VT.

Figure 10 compares the performance of different models in terms of their accuracy in phase-density predictions over 382.14-478.35 K and 35.3-1291.9 bar. Note that the results of CPA EOS model from the work by Tabasinejad *et al*.[11] focuses on the same pressure and temperature ranges. As can be seen from **Figure 10**, although the CPA EOS[12] model can accurately predict the aqueous-phase density, it tends to be less accurate in determining the CO_2-rich-phase density. Overall, the thermodynamic model Case 3-1 (Twu + HV + Abudour *et al*.[10] VT) gives an accuracy comparable to the more complex CPA EOS[12] model.

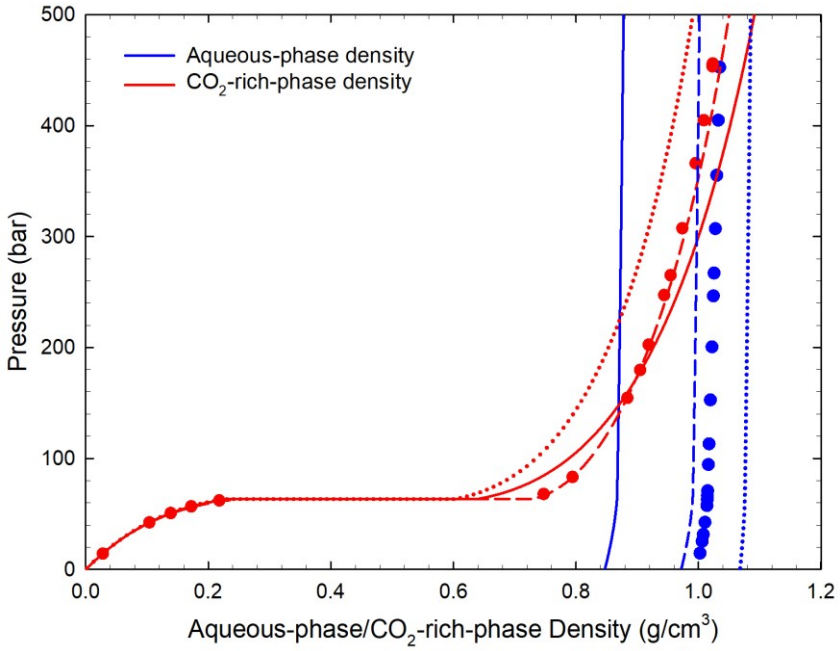

(a)

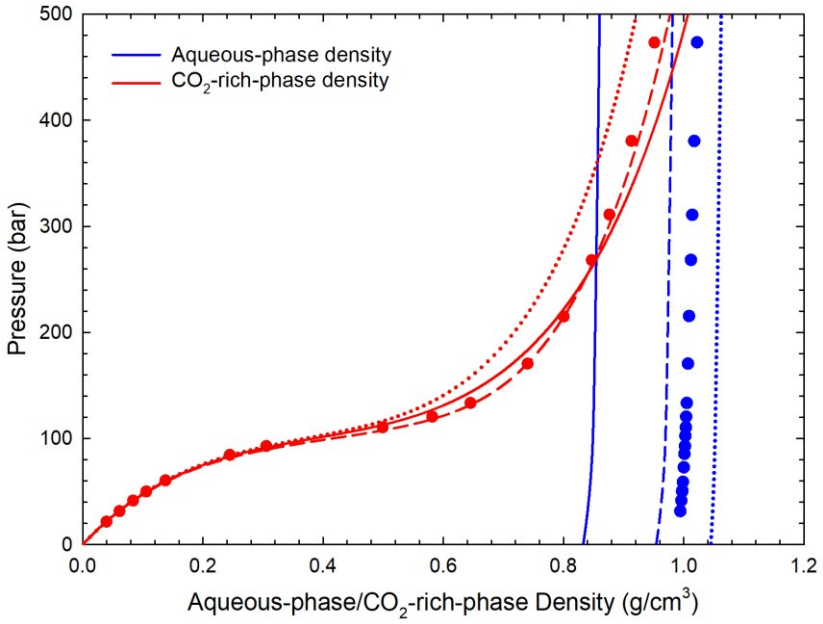

(b)

Figure 7 Predictions of aqueous-phase and CO_2-rich-phase density by Case 3-1 (Abudour *et al.*[10] VT, dashed line), Case 3-2 (Constant VT, dotted line), and Case 3 (base case, solid line) at T=297.8K (a) and T=322.8K (b). The circles are the measured phase-density data from the study by Efika *et al.*[13].

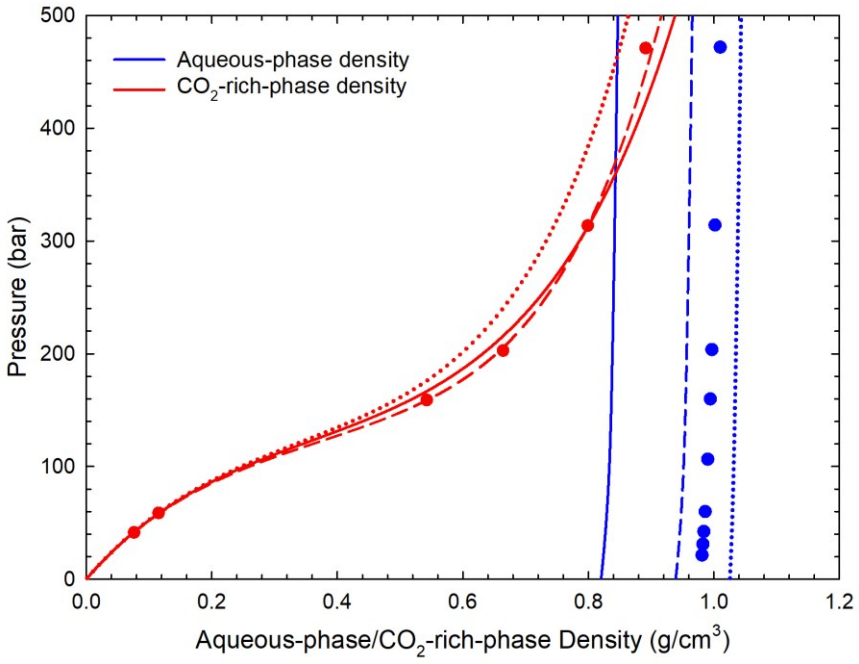

(a)

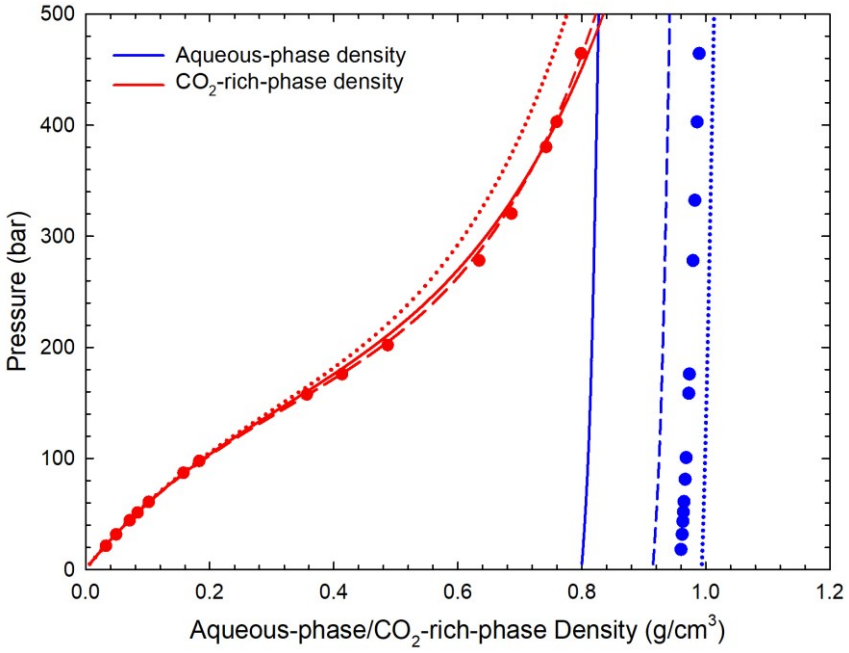

(b)

Figure 8 Predictions of aqueous-phase and CO_2-rich-phase density by Case 3-1 (Abudour *et al.*[10] VT, dashed line), Case 3-2 (Constant VT, dotted line), and Case 3 (base case, solid line) at T=342.8K (a) and T=373K (b). The circles are the measured phase-density data from the study by Efika *et al.*[13].

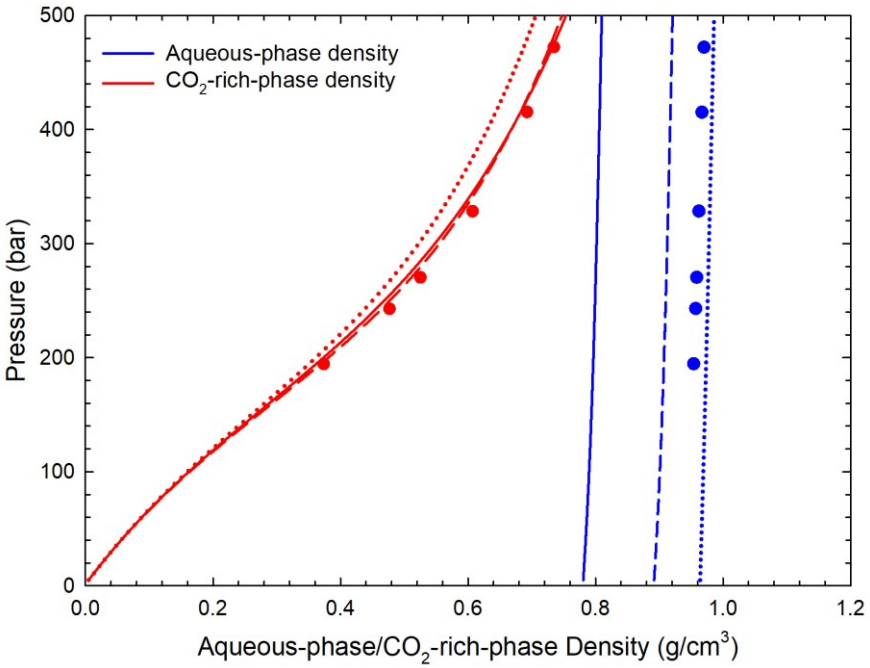

(a)

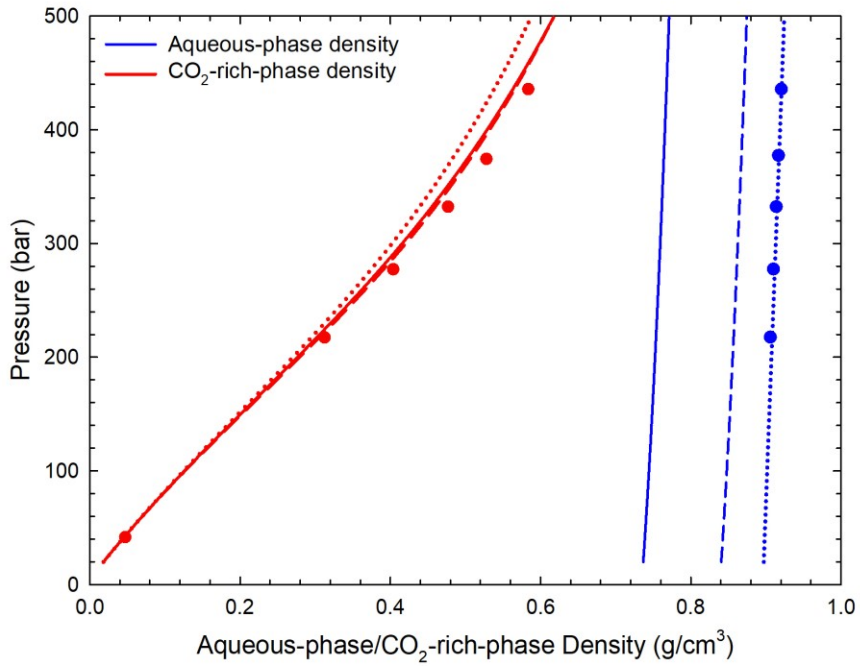

(b)

Figure 9 Predictions of aqueous-phase density and CO_2-rich-phase density by Case 3-1 (Abudour *et al.*[10] VT, dashed line), Case 3-2 (Constant VT, dotted line), and Case 3 (base case, solid line) at T=398.4K (a) and T=448.5K (b). The circles are the measured phase-density data from the study by Efika *et al.*[13].

In addition, according to the study by Aasen *et al.*[7], CPA EOS[12] model yields higher percentage errors in reproducing phase-composition data for CO_2/H_2O mixtures compared with Case 3 (PR EOS + Twu + HV), i.e., 9.5*%AAD* vs. 4.5*%AAD*. Therefore, overall, Case 3-1 (Twu + HV + Abudour *et al.*[10] VT) is a more accurate model in both phase-composition and phase-density predictions for CO_2/H_2O mixtures.

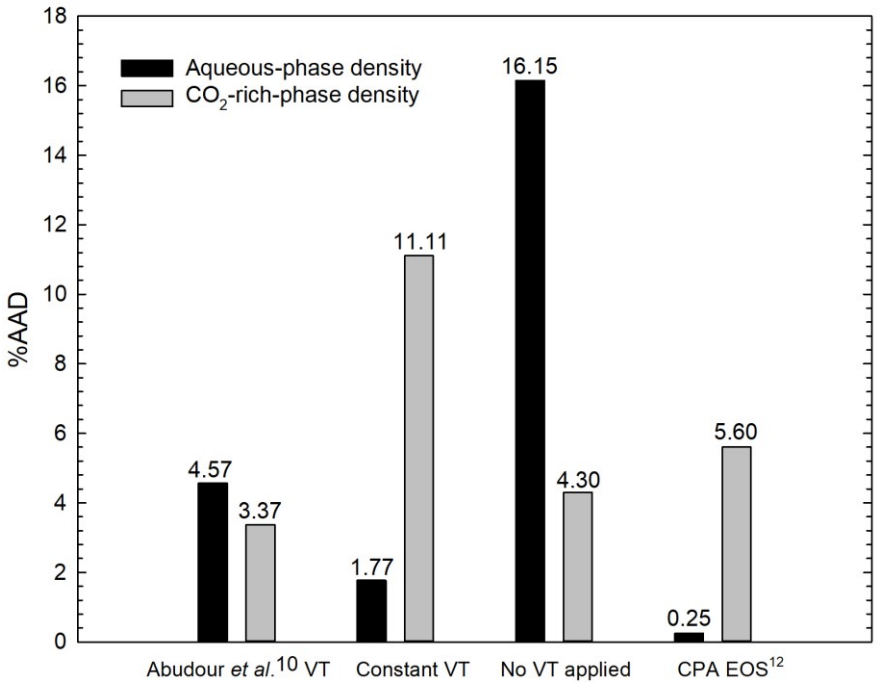

Figure 10 Bar chart plots comparing the *%AAD* in aqueous-phase (black) and CO_2-rich (gray) phase-density predictions by different models over 382.14-478.35 K and 35.3-1291.9 bar. Calculation results by the CPA EOS[12] method are from the study by Tabasinejad *et al.*[11].

3.3 Evaluation of the Newly Proposed IFT Correlation

Results in **Sections 3.1** and **3.2** reveal that the thermodynamic model using PR EOS[14], Twu α function[3], Huron-Vidal mixing rule[5], and Abudour *et al.*[10] VT yields the most accurate estimates on both phase compositions and densities. Therefore, the aforementioned thermodynamic model provides reliable phase-composition and phase-density predictions that can be fed into the proposed IFT correlation.

Mean squared errors (*MSE*), mean absolute errors (*MAE*), *%AAD*, and coefficient of determination (R^2) are used as performance measures. The expressions of *MSE*, *MAE*, and R^2 are as follows:

$$MSE = \frac{1}{NDP}\sum_{i=1}^{NDP}\left(\sigma_{EXP,i} - \sigma_{CAL,i}\right)^2 \tag{55}$$

$$MAE = \frac{1}{NDP}\sum_{i=1}^{NDP}\left|\sigma_{EXP,i} - \sigma_{CAL,i}\right| \tag{56}$$

$$R^2 = 1 - \frac{\sum_{i=1}^{NDP}\left(\sigma_{EXP,i} - \sigma_{CAL,i}\right)^2}{\sum_{i=1}^{NDP}\left(\sigma_{EXP,i} - \bar{\sigma}_{EXP}\right)^2} \tag{57}$$

where σ_{EXP} is the measured IFT data in mN/m; σ_{CAL} is the calculated IFT in mN/m by different correlations; and $\bar{\sigma}_{EXP}$ is the average of the measured IFTs in mN/m.

3.3.1 Performance of Different IFT Correlations

Table 17 shows the details of the different IFT models examined in this study. **Tables 18** and **19** summarize the performance of different correlations in IFT estimations. **Figure 11** shows a parity chart comparing the performance of the different models in IFT estimation when these IFT models are applied to the whole dataset. **Figure 12a** shows a parity chart comparing the performance of Model 3 (Refitted Chen and Yang[15]'s correlation with two coefficient sets), Model 5 (this study), Model 6 (Refitted Hebach *et al.*[16] correlation), and Model 8 (Refitted Chen and Yang[15]'s correlation with one coefficient set) when they are applied to the training dataset, while **Figure 12b** shows another parity chart comparing the performance of these four models when they are applied to the validation dataset. **Tables 18-19** together with **Figures 11-12** demonstrate that the most accurate IFT model is Model 5 proposed in this study, although it only shows a marginal edge over Model 3.

Table 17 Technical characteristics of different IFT models examined in this study.

IFT Model No.	Characteristics
Model 1	Original Parachor model
Model 2	Original Chen and Yang[15]'s correlation with two coefficient sets
Model 3	Refitted Chen and Yang[15]'s correlation with two coefficient sets
Model 4	Original Hebach *et al.*[16] correlation
Model 5	Newly proposed correlation (this study)
Model 6	Refitted Hebach *et al.*[16] correlation
Model 7	Original Chen and Yang[15]'s correlation with one coefficient set
Model 8	Refitted Chen and Yang[15]'s correlation with one coefficient set

Table 18 Summary of the performance of different correlations (original models including Models 1, 2, 4, and 7) in IFT estimations.

Evaluation metrics	Model 1[a]	Model 2[b]	Model 4[c]	Model 7[d]
MSE	264.4564	14.0571	26.6367	29.7705
%AAD	47.0902	9.1794	12.6818	13.3233
MAE	13.7870	2.7889	3.8904	4.2364
R^2	-0.7053	0.8686	0.8568	0.8399

a, b, c, and d: No refitted coefficients are applied in these models. Instead, we directly apply these models in IFT calculations. Thus, it is not necessary to distinguish between training and validation datasets.

Table 19 Summary of the performance of different correlations (refitted or newly proposed models including Model 3, 5, 6, and 8) in IFT estimations.

Evaluation metrics		Model 3	Model 5	Model 6	Model 8
Training dataset	*MSE*	10.7586	8.3475	18.2784	26.0441
	%AAD	7.5218	6.6893	10.6901	11.4002
	MAE	2.4232	2.1311	3.2532	3.8349
	R^2	0.9416	0.9547	0.9008	0.8586
Validation dataset	*MSE*	12.5868	12.9087	18.2676	30.5502
	%AAD	8.8812	8.8684	11.6494	13.3408
	MAE	2.6446	2.6064	3.4174	4.1864
	R^2	0.9116	0.9325	0.9044	0.8402
Overall	*MSE*	11.2030	10.7878	18.2758	27.1388
	%AAD	7.8520	7.7683	10.9231	11.8716
	MAE	2.4770	2.3586	3.2931	3.9203
	R^2	0.9372	0.9420	0.9017	0.8541

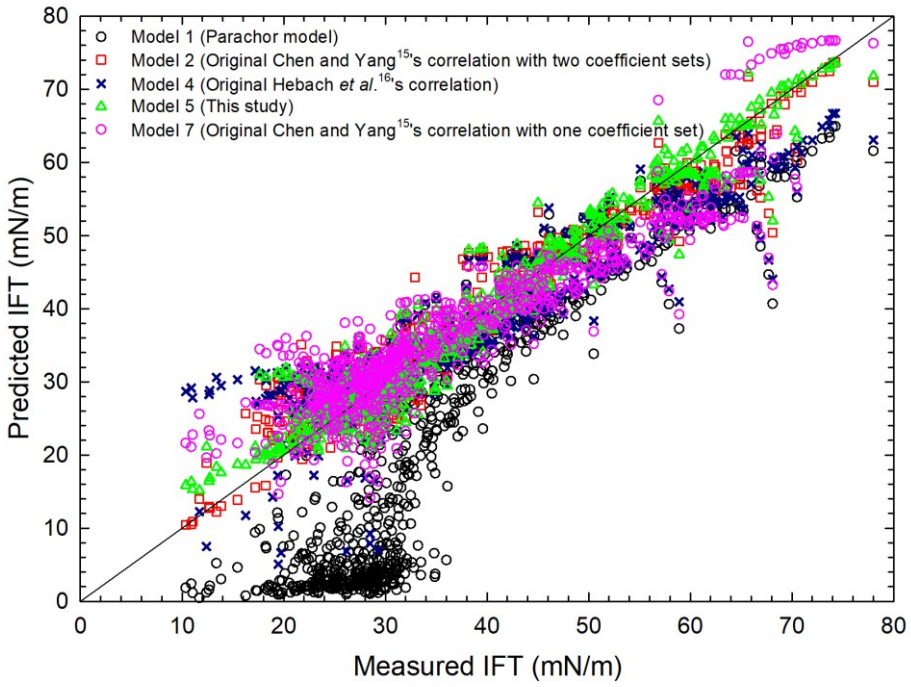

Figure 11 Comparison between the measured IFTs (i.e., the whole dataset) and predicted IFTs by Model 1 (Parachor model), Model 2 (original Chen and Yang[15]'s correlation with two coefficient sets), Model 4 (original Hebach *et al.*[16] correlation), Model 5 (this study), and Model 7 (original Chen and Yang[15]'s correlation with one coefficient set).

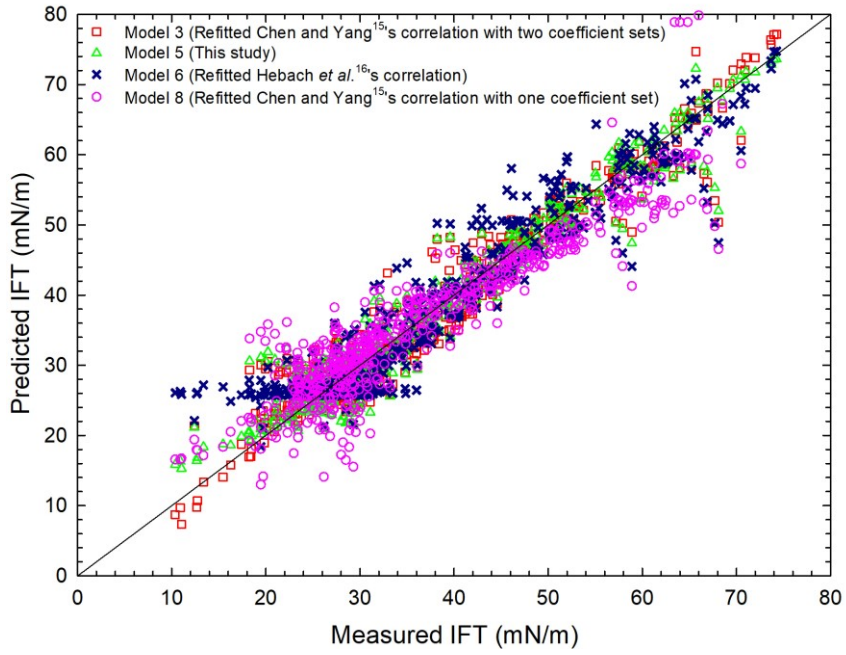

(a)

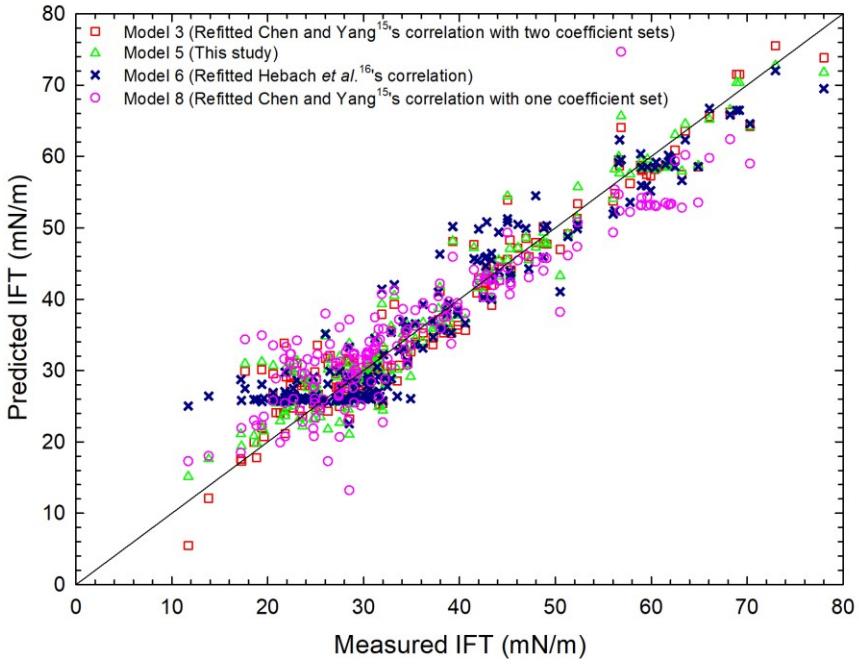

(b)

Figure 12 Comparison between the measured and estimated IFTs by Model 3 (Refitted Chen and Yang[15]'s correlation with two coefficient sets), Model 5 (this study), Model 6 (Refitted Hebach *et al.*[16] correlation), and Model 8 (Refitted Chen and Yang[15]'s correlation with one coefficient set): (a) training dataset; (b): validation dataset.

Figures 13-15 visually compare the measured IFTs vs. pressure and the calculated ones by different IFT models at selected temperatures. As shown in these plots, in general, Model 5 proposed in this study outperforms other empirical correlations over a wide range of temperatures and pressures. It can be also observed from these plots that breaking points appear in the predicted IFT curves at p=73.8 bar by both Model 2 (original Chen and Yang[15]'s correlation with two coefficient sets) and Model 3 (Refitted Chen and Yang[15]'s correlation with two coefficient sets). Such discontinuous IFT prediction can be attributed to the fact that two different sets of coefficients are adopted under the conditions of $p \leq 73.8$ bar and $p > 73.8$ bar, respectively, in Chen and Yang[15]'s correlation. Although using one coefficient in Chen and Yang's correlation (e.g. Models 7 and 8) can avoid such discontinuous IFT predictions, it yields larger percentage errors. Therefore, Model 5 (this study) is the optimal model for IFT predictions for CO_2/H_2O mixtures over a wide range of temperatures and pressures.

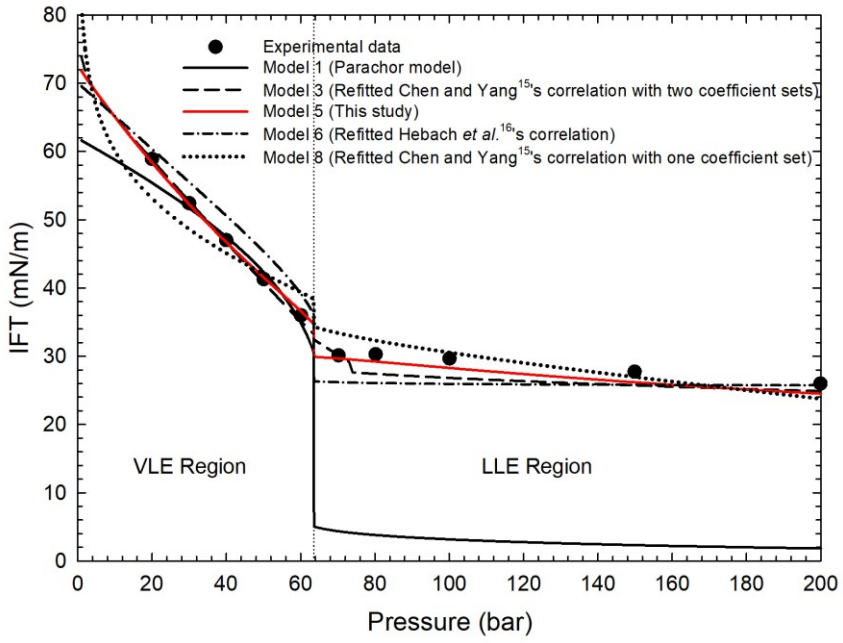

(a)

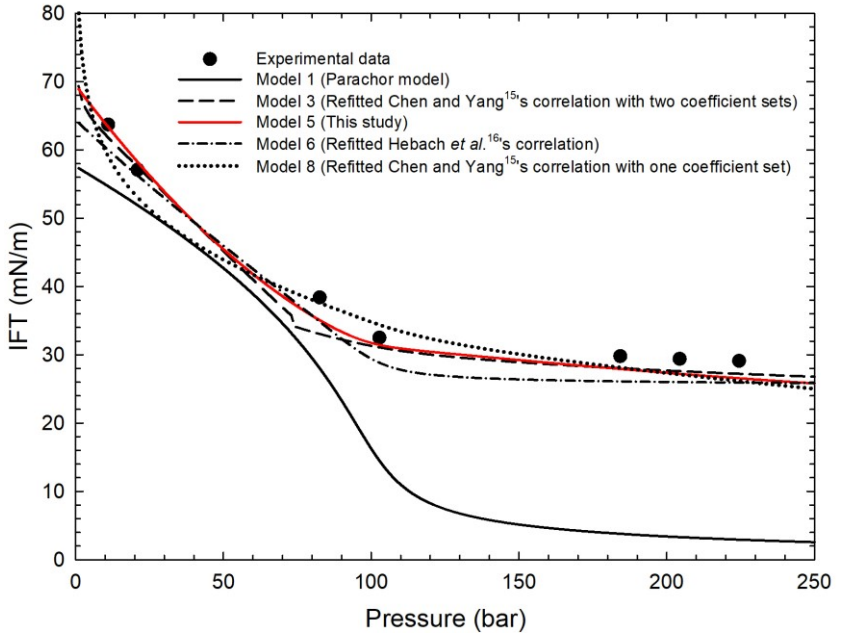

(b)

Figure 13 IFT predictions at T=297.9 K (a) and T=322.8 K (b) by different models. At T=297.9 K, VLE is transformed to LLE at p=64 bar. Model 1 (Parachor model) shows a more deteriorating performance when the vapor CO_2-rich phase changes to a liquid phase. Experimental data are from the studies by Kvamme *et al.*[17] and Georgiadis *et al.*[18].

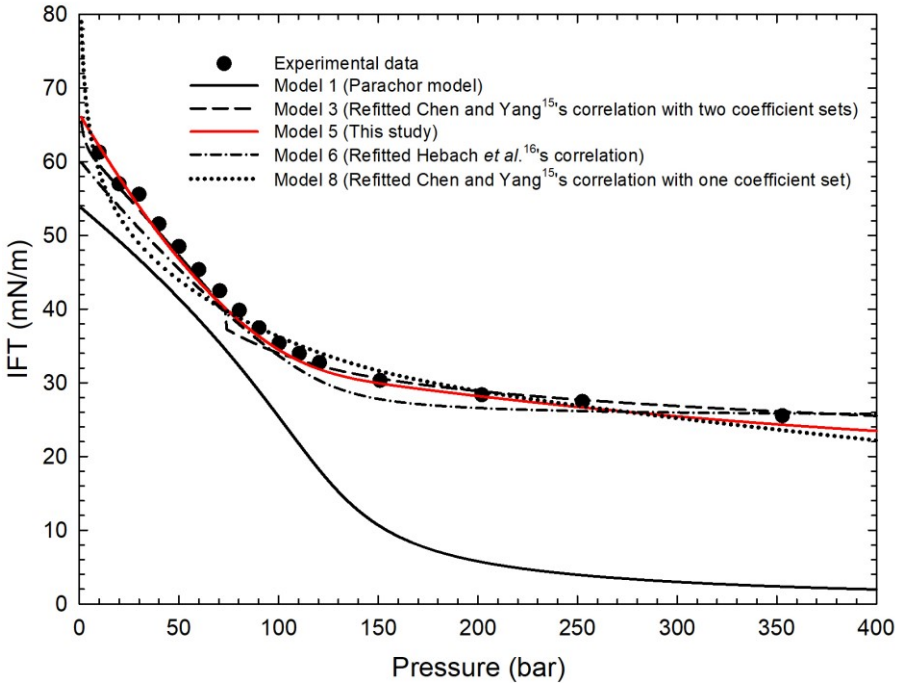

(a)

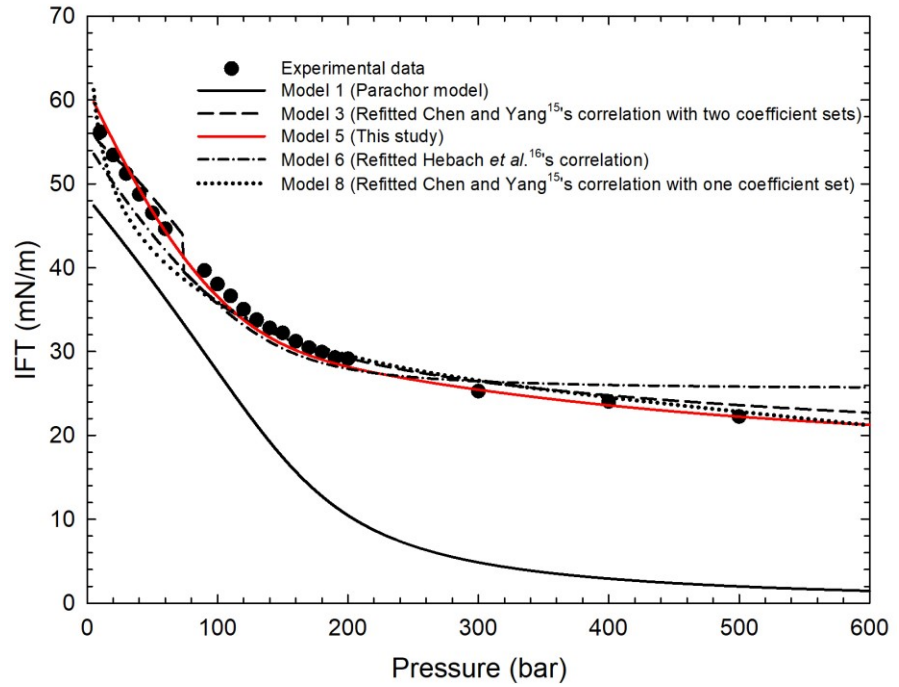

(b)

Figure 14 IFT predictions at $T = 343.3$ K (a) and $T = 374.3$ K (b) by different models. Experimental data are from the study by Georgiadis *et al*.[18].

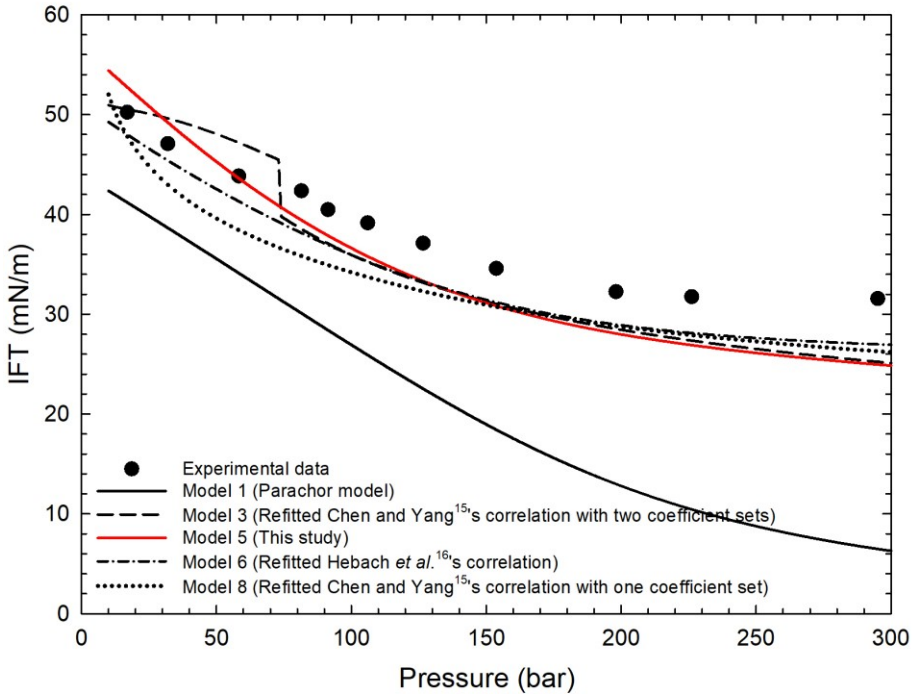

(a)

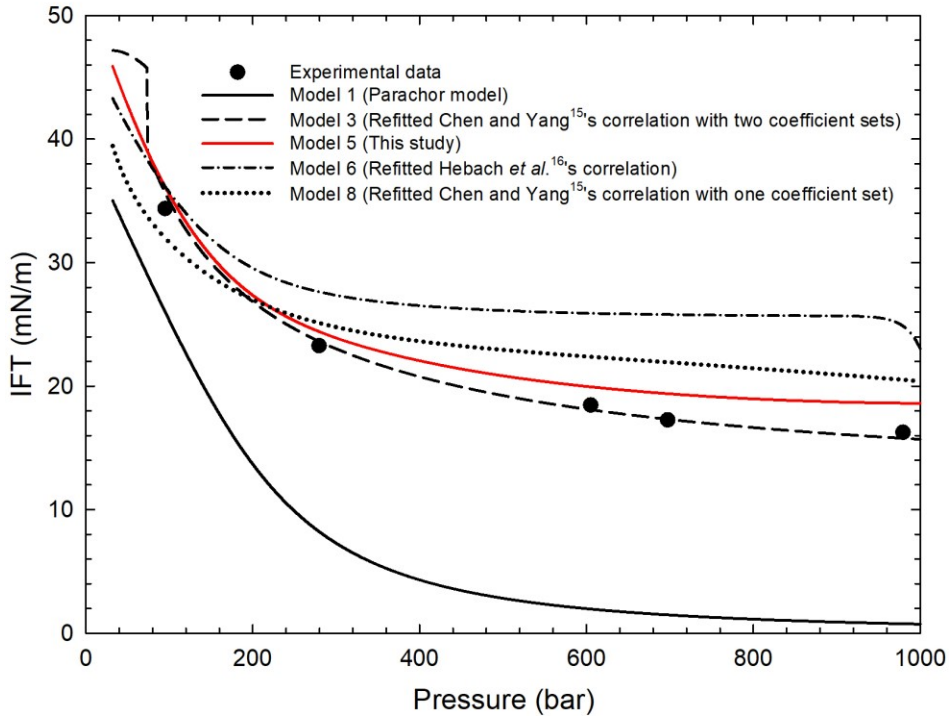

(b)

Figure 15 IFT calculation results at T=398.15 K (a) and T=422.04 K (b) by different models. Experimental data are from the studies by Liu *et al.*[19] and Shariat *et al.*[20].

Figure 16 illustrates how the IFTs predicted by Model 5 (this study) vary with pressure at different temperatures. It can be observed from **Figure 16** that the new IFT correlation provides smooth and consistent IFT predictions at different pressures and temperatures. It is interesting to observe from **Figure 16a** that when pressure is less than around 15 bar and the temperature is between 278.15-368.15 K, an increase in temperature leads to a decrease in the predicted IFT under the same pressure. In comparison, when pressure is larger than around 15 bar, an increase in temperature leads to an increase in the predicted IFT. At higher temperatures of 378.15-478.15 K, an increase in temperature always results in a decline in the predicted IFT under the same pressure, as seen in **Figure 16b**. Most of the measured IFTs documented in the literature follow this trend[16-30] except for the studies by Bachu and Bennion[31] and Bikkina *et al*.[32], i.e., an increase in temperature leads to an increase in IFT at a temperature range of 373.15-398.15 K in the study by Bachu and Bennion[31], and an increase in temperature leads to an increase in IFT over 298.15.15-333.15 K in the study by Bikkina *et al.*[32]. Again, the sharp drops in the IFTs at lower temperatures (where CO_2 remains subcritical) are due to the transformation of VLE to LLE.

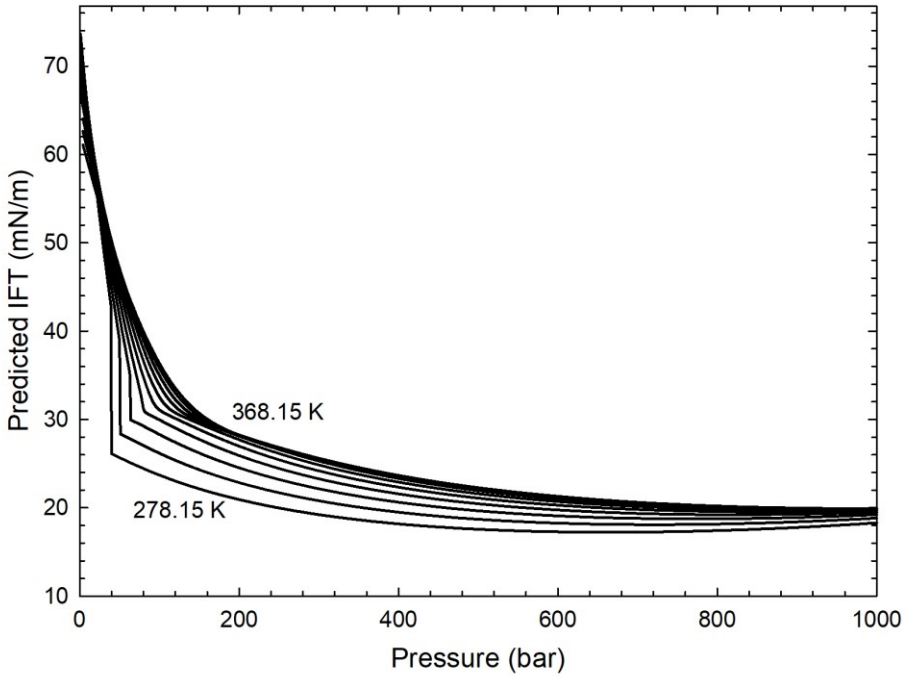

(a)

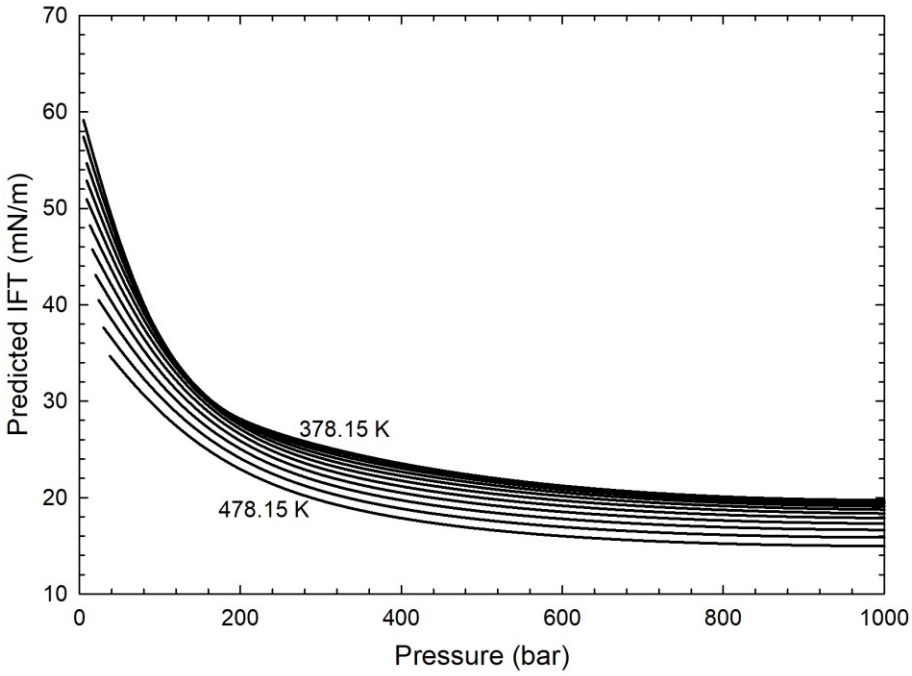

(b)

Figure 16 Plots of predicted IFTs vs. pressure by the newly proposed IFT correlation Model 5 at the temperature ranges of 278.15-368.15 K (a) and 378.15-478.15 K (b). The curves are plotted with an interval of 10 K.

3.3.2 Statistical Significance Tests of IFT Correlations

As shown in **Table 18**, the *%AAD*s yielded by Model 3 and Model 5 are on the same scale. Therefore, it is necessary to conduct statistical significance tests to check if the marginal edge of Model 5 over Model 3 is statistically significant. **Figure 17** shows the frequency distribution of the differences between the measured IFT data (i.e., the whole dataset including 778 data points) and calculated ones by Model 3 (refitted Chen and Yang[15]'s correlation with two coefficient sets), while **Figure 18** shows the same information for Model 5. As can be seen from **Figures 17** and **18**, the distribution of the deviations generated by the two models can be considered to follow Gaussian distributions. As such, paired one-tailed t-tests are applied as the statistical significance test method[33]. The t-test results are summarized in **Table 20**.

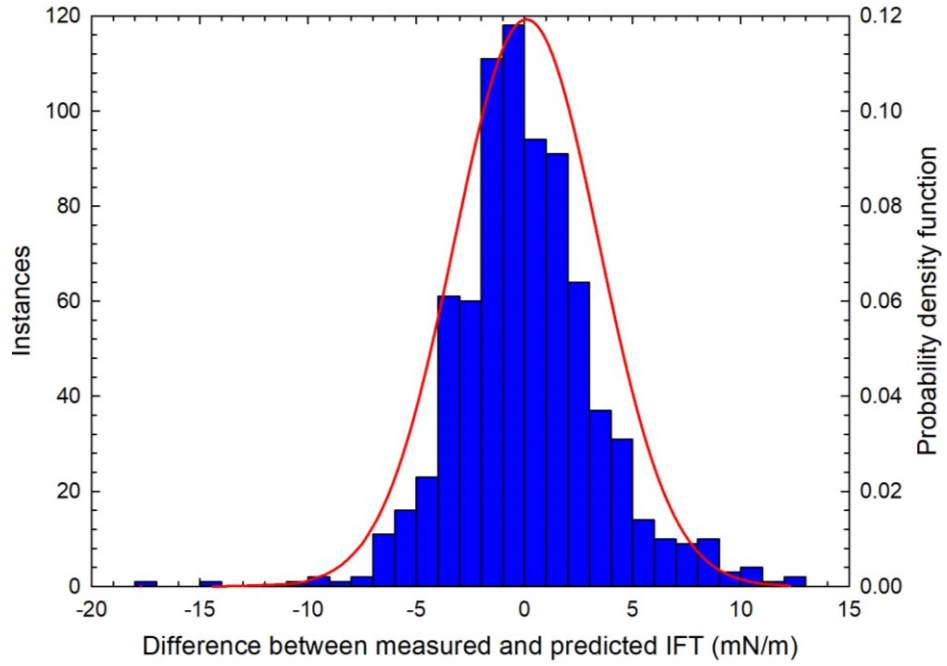

Figure 17 Frequency distribution of the differences between the measured IFT data (i.e., the whole dataset including 778 data points) and calculated ones by Model 3 (refitted Chen and Yang[15]'s correlation with two coefficient sets). Blue columns are instances, and the red curve is probability density function curve which follows Gaussian distribution with $\mu = 0.0941$ and $\sigma^2 = 3.3457$.

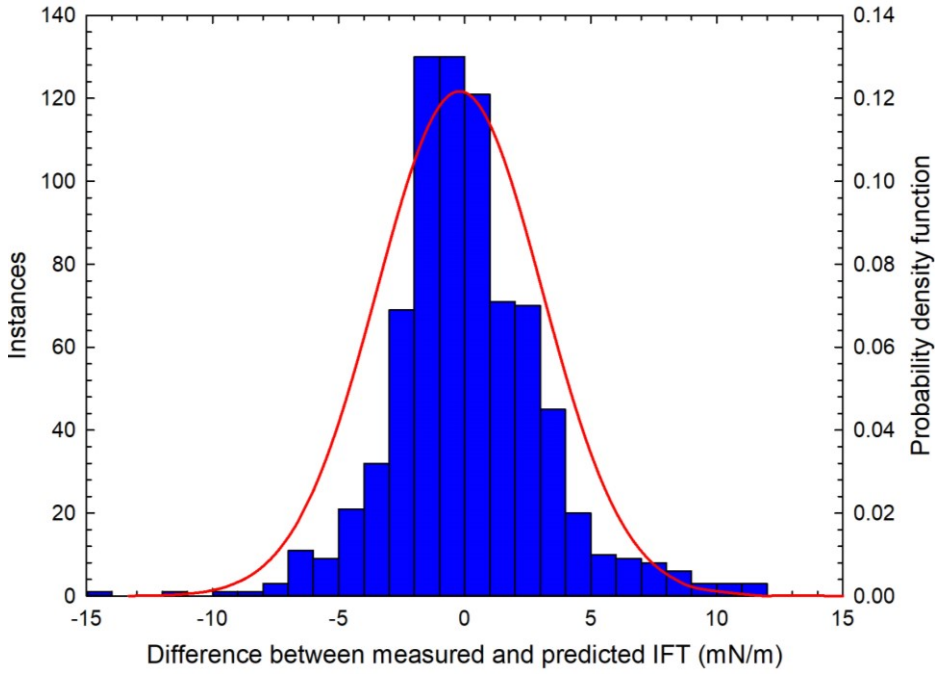

Figure 18 Frequency distribution of the difference between the measured IFT data (i.e., the whole dataset including 778 data points) and calculated ones by Model 5. Blue columns are instances, and the red curve is probability density function curve which follows Gaussian distribution with μ = -0.2051 and σ^2 = 3.2781.

P-value is used to check if one model is better than another one. Typically, the significance threshold α is 0.05; when P>α, two models have the same performance. In contrast, when P≤α, it is reasonable to say that one model is significantly better than another one[33].

As shown in **Table 20**, the P-value of Model 2 (the original Chen and Yang[15]'s correlation with two coefficient sets) and Model 3 (refitted Chen and Yang[15]'s correlation with two coefficient sets) is lower than 0.05; therefore, it is reasonable to say that Model 3 outperforms Model 2 statistically. Similarly, since the P-value for Model 2 and Model 5 is lower than 0.05, Model 5 outperforms Model 2. In addition, because the P-value for Model 3 and Model 5 is lower than 0.05, Model 5 outperforms Model 3. It is thus safe to conclude that the newly proposed IFT model outperforms the refitted Chen and Yang[15]'s model with two coefficient sets. In addition, the new model does not give discontinuous IFT predictions, while Chen and Yang[15]'s IFT model bears such issue.

Table 20 Paired one-tailed t-test results on three IFT models.

Model #1	Model #2	P-value	Winning model
Model 2	Model 3	0.0001	Model 3
Model 2	Model 5	0.0013	Model 5
Model 3	Model 5	0.0069	Model 5

References

[1] Lemmon, E.W.; McLinden, M.O.; Friend, D.G. Thermophysical properties of fluid systems, in: P.J. Linstrom, W.G. Mallard (Eds.). NIST Chemistry WebBook, NIST Standard Reference Database Number 69, National Institute of Standards and Thecnology, Gaithersburg, MD 20899, 2011.

[2] Gasem, K.A.M.; Gao, W.; Pan, Z.; Robinson, R.L. A modified temperature dependence for the Peng-Robinson equation of state. *Fluid Phase Equilib*. **2001**, 181, 113-125.

[3] Twu, C.H.; Bluck, D.; Cunningham, J.R.; Coon, J.E. A cubic equation of state with a new alpha function and a new mixing rule. *Fluid Phase Equilib*. **1991**, 69, 33-50.

[4] van der Waals, J.D. Continuity of the gaseous and liquid state of matter. 1873.

[5] Huron, M.J.; Vidal, J. New mixing rules in simple equations of state for representing vapor-liquid equilibria of strongly non-ideal mixtures. *Fluid Phase Equilib*. **1979**, 3, 255-271.

[6] Abudour, A.M.; Mohammad, S.A.; Gasem, K.A.M. Modeling high-pressure phase equilibria of coalbed gases/water mixtures with the Peng-Robinson equation of state. *Fluid Phase Equilib*. **2012**, 319, 77-89.

[7] Aasen, A.; Hammer, M.; Skaugen, G.; Jakobsen, J.P.; Wilhelmsen, Ø. Thermodynamic models to accurately describe the PVTxy-behavior of water/carbon dioxide mixtures. *Fluid Phase Equilib*. **2017**, 442, 125-139.

[8] Briones, J.A.; Mullins, J.C.; Thies, M.C. Ternary phase equilibria for acetic acid-water mixtures with supercritical carbon dioxide. *Fluid Phase Equilib*. **1987**, 36, 235-246.

[9] Gillepsie, P.C.; Wilson, G.M. Vapor-liquid and liquid-liquid equilibria: water-methane, water-carbon dioxide, water-hydrogen sulfide, water-n-pentane, water-methane-n-pentane. Research report RR-48, Gas Processors Association, Tulsa Okla., April 1982.

[10] Abudour, A.M.; Mohammad, S.A.; Robinson R.L.; Gasen, K.A.M. Volume-translated Peng-Robinson equation of state for liquid densities of diverse binary mixtures. *Fluid Phase Equilib*. **2013**, 349, 37-55.

[11] Tabasinejad, F.; Barzin, Y.; Moore, G.R.; Mehta, S.A.; Fraassen, K.C.V.; Rushing, J.A.; Newsham, K.E. Water/CO_2 system at high pressure and temperature conditions: measurement and modeling of density in equilibrium liquid and vapor phases. Paper SPE 131636 presented at the SPE EUROPEC/EAGD Annual Conference and Exhibition. Barcelona, Spain, June 14-17, 2010.

[12] Kontogeorgis, G.M.; Voutsas, E.C.; Yakoumis, I.V.; Tassios, D.P. An equation of state for associating fluids. *Ind. Eng. Chem. Res*. **1996**, 35, 4310-4318.

[13] Efika, E.C.; Hoballah, R.; Li, X.; May, E.F.; Nania, M.; Vicente, Y.S., Trusler, J.P.M. Saturated phase densities of (CO_2 + H_2O) at temperatures from (293 to 450) K and pressures up to 64 MPa. *J. Chem. Thermodyn*. **2016**, 93, 347-359.

[14] Peng, D.Y.; Robinson, D.B. A new two-constant equation of state. *Ind. Eng. Chem. Fundamen*. **1976**, 15, 59-64.

[15] Chen, Z.; Yang, D. Correlations/estimation of equilibrium interfacial tension for methane/CO_2-water/brine systems based on mutual solubility. *Fluid Phase Equilib*. **2019**, 483, 197-208.

[16] Hebach, A.; Oberhof, A.; Dahmen, N.; Kögel, A.; Ederer, H.; Dinjus, E. Interfacial tension at elevated pressures – measurements and correlations in the water + carbon dioxide system. *J. Chem. Eng. Data*. **2002**, 47, 1540-1546.

[17] Kvamme, B.; Kuznetsova, T.; Hebach, A.; Oberhof, A.; Lunde, E. Measurements and modelling of interfacial tension for water + carbon dioxide systems at elevated pressures. *Comput. Mater. Sci*. **2007**, 38, 506-513.

[18] Georgiadis, A.; Maitland, G.; Trusler, J.P.; Bismarck, A. Interfacial tension measurements of the (H_2O + CO_2) system at elevated pressures and temperatures. *J. Chem. Eng. Data*. **2010**, 55, 4168-4175.

[19] Liu, Y.; Li, H.; Okuno, R. Measurements and modeling of interfacial tension for CO_2/CH_4/brine systems under reservoir conditions. *Ind. Eng. Chem. Res*. **2016**, 55, 12358-12375.

[20] Shariat, A.; Moore, R.G.; Mehta, S.A.; Fraassen, K.C.; Newsham, K.E.; Rushing, J.A. Laboratory measurements of CO_2-H_2O interfacial tension at HP/HT conditions: implications for CO_2 sequestration in deep aquifers. Paper CMTC 150010 presented at Carbon Management Technology Conference. Orlando, Florida, USA, February 7-9, 2012.

[21] Chiquet, P.; Daridon, J.; Broseta, D.; Thibeau, S. CO_2/water interfacial tensions under pressure and temperature conditions of CO_2 geological storage. *Energy Convers. Manag*. **2007**, 48, 736-744.

[22] Heuer, G.J. Interfacial tension of water against hydrocarbons and other gases and adsorption of methane on solids at reservoir temperatures and pressures. PhD Dissertation, Univ. of Texas at Austin, Austin, Texas. 1957.

[23] Hough, E.W.; Henuer, G.J.; Walker, J.W. An improved pendant drop, interfacial tension apparatus and data for carbon dioxide and water. *Pet. Trans. AIME.* **1969**, 2052, 216, 469-472.

[24] Chun, B.S.; Wilkinson, G.T. Interfacial tension in high-pressure carbon dioxide mixtures. *Ind. Eng. Chem. Res*. **1995**, 34, 4371-4377.

[25] Da Rocha, S.R.P.; Harrison, K.L.; Johnston, K.P. Effect of surfactants on the interfacial tension and emulsion formation between water and carbon dioxide. *Langmuir*. **1999**, 15, 419-428.

[26] Park, J.Y.; Lim, J.S.; Yoon, C.H.; Lee, C.H.; Park, K.P. Effect of a fluorinated Sodium Bis (2-ethylhexyl) sulfosuccinate (aerosol-OT, AOT) analogue surfactant on the interfacial tension of CO_2 + water and CO_2 + Ni-Plating solution in near- and supercritical CO_2. *J. Chem. Eng. Data*. **2005**, 50, 299-308.

[27] Akutsu, T.; Yamaji. Y.; Yamaguchi, H.; Watanabe, M.; Smith, R.; Inomata, H. Interfacial tension between water and high pressure CO_2 in the presence of hydrocarbon surfactants. *Fluid Phase Equilib*. **2007**, 257, 163-168.

[28] Chalbaud, C.; Robin, M.; Lombard, J.M.; Martin, F.; Egermann, P.; Bertin, H. Interfacial tension measurements and wettability evaluation for geological CO_2 storage. *Adv. Water Resour*. **2009**, 32, 98-109.

[29] Khosharay, S.; Varaminian, F. Experimental and modeling investigation on surface tension and surface properties of (CH_4 + H_2O), (C_2H_6 + H_2O), (CO_2 + H_2O) and (C_3H_8 + H_2O) from 284.15K to 312,15K and pressures up to 60bar. *Int. J. Refrig*. **2014**, 47, 26-35.

[30] Pereira, L.; Chapoy, A.; Burgass, R.; Oliveira, M.B.; Coutinho, J.; Tohidi, B. Study of the impact of high temperatures and pressures on the equilibrium densities and interfacial tension of the carbon dioxide/water system. *J. Chem. Thernodyn*. **2016**, 93, 404-415.

[31] Bachu, S.; Bennion, D.B. Interfacial tension between CO_2, freshwater, and brine in the range of pressure from (2 to 27) MPa, temperature from (20 to 125) ^oC, and water salinity from (0 to 334000) mg • L^{-1}. *J. Chem. Eng. Data*. **2009**, 54, 765-775.

[32] Bikkina, P.K.; Shoham, O.; Uppaluri, R. Equilibrated interfacial tension data of the CO_2-water system at high pressures and moderate temperatures. *J. Chem. Eng. Data*. **2011**, 56, 3725-3733.

[33] Japkowicz, N.; Shah, M. Evaluating learning algorithms – a classification perspective. Cambridge University Press, 2011.

CHAPTER 4 CONCLUSIONS AND RECOMMENDATIONS

4.1 Conclusions

The objective of this study is to screen and develop reliable models for describing the VLE, LLE, phase density, and IFT of CO_2/H_2O mixtures. Based on the comparison between the experimental data and the calculated ones from different models, we can reach the following conclusions:

(1) The most accurate method to represent CO2/H2O VLE and LLE is PR EOS[1], Twu α function[2], and Huron-Vidal mixing rule[3], which yields 6.52*%AAD* and 2.88*%AAD* in reproducing the measured CO_2/H_2O phase-composition data and phase-density data over a temperature range of 278-378.15 K and 278-478.35 K and over a pressure range of 6.9-709.3 bar and 278-478.35 bar, respectively;

(2) Applying either constant or Abudour *et al*.[4] VT method can significantly improve aqueous-phase density calculations. In addition, when the temperature is higher than 373 K, constant VT method can yield lower error in reproducing measured phase-density data than Abudour *et al*.[4] VT method;

(3) Constant VT method cannot improve the prediction accuracy of CO_2-rich-phase density. Abudour *et al*.[4] VT method can slightly improve CO_2-rich-phase density predictions, but such improvement is more obvious at low to moderate temperature conditions;

(4) The new IFT correlation based on the aforementioned PR EOS model outperforms other empirical correlations with an overall 7.77*%AAD* in reproducing measured IFT data of CO_2/H_2O mixtures. The new IFT correlation is only slightly more accurate than the refitted Chen and Yang[5]'s correlation with two coefficient sets. But the new correlation yields smooth IFT predictions, avoiding the issue of discontinuous IFT predictions yielded by Chen and Yang[5]'s correlation.

4.2 Recommendations

More experimental phase-density data of CO_2/H_2O mixtures over a wide range of temperatures and pressures are needed to further examine the performance of the PR EOS[1], Twu α function[2], Huron-Vidal mixing rule[3], and Abudour *et al*.[4] VT model. We currently lack the experimental data at high-pressure and low-temperature (i.e., $p > 300$ bar and 285 K < T < 300 K) conditions. In addition, the aforementioned thermodynamic model yields accurate results in reproducing the measured phase-density data at low-to-moderate temperatures ($T < 373.15$ K) but yields larger percentage errors at high temperatures ($T > 373.15$ K); therefore, some modifications to Abudour *et al*.[4] VT model could be further made to well capture the variation trend of phase densities of CO_2/H_2O mixtures at high temperatures. With regards to the IFT modeling, more experimental data at high pressures and low temperatures (i.e., $p > 300$ bar and 285 K < T < 300 K) are needed to further examine the performance of the newly proposed IFT correlation. Last but not least, water salinity poses an important effect on the phase behavior and IFT of CO_2/H_2O mixtures, which is, however, not considered in this thesis. Future modeling efforts should take water salinity into account.

References

[1] Peng, D.Y.; Robinson, D.B. A new tow-constant equation of state. *Ind. Eng. Chem. Fundamen.* **1976**, 15, 59-64.

[2] Twu, C.H.; Bluck, D.; Cunningham, J.R.; Coon, J.E. A cubic equation of state with a new alpha function and a new mixing rule. *Fluid Phase Equilib*. **1991**, 69, 33-50.

[3] Huron, M.J.; Vidal, J. New mixing rules in simple equations of state for representing vapor-liquid equilibria of strongly non-ideal mixtures. *Fluid Phase Equilib*. **1979**, 3, 255-271.

[4] Abudour, A.M.; Mohammad, S. A.; Robinson Jr, R. L.; Khaled, A. M. G. Volume-translated Peng-Robinson equation of state for liquid densities of diverse binary mixtures. *Fluid Phase Equilib*. **2013**, 349, 37-55.

[5] Chen, Z.; Yang, D. Correlations/estimation of equilibrium interfacial tension for methane/CO_2-water/brine systems based on mutual solubility. *Fluid Phase Equilib*. **2019**, 483, 197-208.

BIBLIOGRAPHY

Aalto, M.; Keskinen, K.I.; Aittamaa, J.; Liukkonen, S. An improved correlation for compressed liquid densities of hydrocarbons. Part 2. Mixtures. *Fluid Phase Equilib*. **1996**, 114, 21-35.

Aasen, A.; Hammer, M.; Skaugen, G.; Jakobsen, J.P.; Wilhelmsen, Ø. Thermodynamic models to accurately describe the PVTxy-behavior of water/carbon dioxide mixtures. *Fluid Phase Equilib*. **2017**, 442, 125-139.

Abudour, A.M.; Mohammad, S.A.; Robinson Jr, R.L.; Khaled, A.M.G. Volume-translated Peng-Robinson equation of state for saturated and single-phase liquid densities. *Fluid Phase Equilib*. **2012**, 335, 74-87.

Abudour, A.M.; Mohammad, S.A.; Robinson Jr, R.L.; Khaled, A.M.G. Volume-translated Peng-Robinson equation of state for liquid densities of diverse binary mixtures. *Fluid Phase Equilib*. **2013**, 349, 37-55.

Abudour, A.M.; Sayee, A.M.; Khaled, A.M.G. Modeling high-pressure phase equilibria of coalbed gases/water mixtures with the Peng–Robinson equation of state. *Fluid Phase Equilib.* **2012**, 319, 77-89.

Akutsu, T.; Yamaji. Y.; Yamaguchi, H.; Watanabe, M.; Smith, R.; Inomata, H. Interfacial tension between water and high pressure CO_2 in the presence of hydrocarbon surfactants. *Fluid Phase Equilib*. **2007**, 257, 163-168.

Bachu, S.; Bennion, D.B. Interfacial tension between CO_2, freshwater, and brine in the range of pressure from (2 to 27) MPa, temperature from (20 to 125) ºC, and water salinity from (0 to 334000) mg • L^{-1}. *J. Chem. Eng. Data*. **2009**, 54, 765-775.

Bikkina, P.K.; Shoham, O.; Uppaluri, R. Equilibrated interfacial tension data of the CO_2-water system at high pressures and moderate temperatures. *J. Chem. Eng. Data*. **2011**, 56, 3725-3733.

Briones, J.A.; Mullins, J.C.; Thies, M.C.; Kim, B.U. Ternary phase equilibria for acetic acid-water mixtures with supercritical carbon dioxide. *Fluid Phase Equilib*. **1987**, 36, 235-246.

Chalbaud, C.; Robin, M.; Lombard, J.-M.; Martin, F.; Egermann, P.; Bertin, H. Interfacial tension measurements and wettability evaluation for geological CO_2 storage. *Adv. Water Resour*. **2009**, 32, 98-109.

Chen, Z.; Yang, D. Correlations/estimation of equilibrium interfacial tension for methane/CO_2-water/brine systems based on mutual solubility. *Fluid Phase Equilib*. **2019**, 483, 197-208.

Chiquet, P.; Daridon, J.; Broseta, D.; Thibeau, S. CO_2/water interfacial tensions under pressure and temperature conditions of CO_2 geological storage. *Energy Convers. Manag*. **2007**, 48, 736-744.

Chun, B.S.; Wilkinson, G.T. Interfacial tension in high-pressure carbon dioxide mixtures. *Ind. Eng. Chem. Res*. **1995**, 34, 4371-4377.

Da Rocha, S.R.P.; Harrison, K.L.; Johnston, K.P. Effect of surfactants on the interfacial tension and emulsion formation between water and carbon dioxide. *Langmuir*. **1999**, 15, 419-428.

Dohrn, R.; Bünz, A.P.; Devlieghere, F.; Thelen, D. Experimental measurements of phase equilibria for ternary and quaternary systems of glucose, water, CO_2 and ethanol with a novel apparatus. *Fluid Phase Equilib*. **1993**, 83, 149-158.

D'Souza, R.; Patrick, J.R.; Teja, A.S. High pressure phase equilibria in the carbon dioxide – n-hexadecane and carbon dioxide-water systems. *Can. J. Chem. Eng*. **1988**, 66, 319-323.

Efika, E.C.; Hoballah, R.; Li, X.; May, E.F.; Nania, M.; Vicente, Y.S.; Trusler, J.P.M. Saturated phase densities of (CO_2 + H_2O) at temperatures from (293 to 450) K and pressures up to 64 MPa. *J. Chem. Thermodyn*. **2016**, 93, 347-359.

Gasem, K.A.M.; Gao, W.; Pan, Z.; Robinson, R.L. A modified temperature dependence for the Peng-Robinson equation of state. *Fluid Phase Equilib*. **2001**, 181, 113-125.

Georgiadis, A.; Maitland, G.; Trusler, J.P.; Bismarck, A. Interfacial tension measurements of the (H_2O + CO_2) system at elevated pressures and temperatures. *J. Chem. Eng. Data*. **2010**, 55, 4168-4175.

Gernert. J.; Span. R. EOS-CG: a Helmholtz energy mixture model for humid gases and CCS mixtures. *J. Chem. Thermodyn*. **2016**, 93, 274-293.

Gillepsie, P.C.; Wilson, G.M. Vapor-liquid and liquid-liquid equilibria: water-methane, water-carbon dioxide, water-hydrogen sulfide, water-n-pentane, water-methane-n-pentane. Research report RR-48, Gas Processors Association, Tulsa Okla., April 1982.

Gross, J.; Sadowski, G. Perturbed-chain SAFT: an equation of state based on a perturbation theory for chain molecules. *Ind. Eng. Chem. Res*. **2001**, 40, 1244-1260.

Hebach, A.; Oberhof, A.; Dahmen, N.; Kögel, A.; Ederer, H.; Dinjus, E. Interfacial tension at elevated pressures – measurements and correlations in the water + carbon dioxide system. *J. Chem. Eng. Data*. **2002**, 47, 1540-1546.

Hebach, A.; Oberhof, A.; Dahmen, N. Density of water plus carbon dioxide at elevated pressures: measurements and correlation. *J. Chem. Eng. Data*. **2004**, 49, 950-953.

Heuer, G.J. Interfacial tension of water against hydrocarbons and other gases and adsorption of methane on solids at reservoir temperatures and pressures. PhD Dissertation, Univ. of Texas at Austin, Austin, Texas. 1957.

Hough, E.W.; Henuer, G.J.; Walker, J.W. An improved pendant drop, interfacial tension apparatus and data for carbon dioxide and water. *Pet. Trans. AIME.* **1969**, 216, 469-472.

Hu, J.; Duan, Z.; Zhu, C.; Chou, I. PVTx properties of the CO_2-H_2O and CO_2-H_2O-NaCl systems below 647 K: assessment of experimental data and thermodynamic models. *Chem. Geol*. **2007**, 238, 249-267.

Huron, M.J.; Vidal, J. New mixing rules in simple equations of state for representing vapor-liquid equilibria of strongly non-ideal mixtures. *Fluid Phase Equilib*. **1979**, 3, 255-271.

Japkowicz, N.; Shah, M. Evaluating learning algorithms – a classification perspective. Cambridge University Press, 2011.

Jhaveri, B.S.; Youngren, G.K. Three-parameter modification of the Peng-Robinson equation of state to improve volumetric predictions. *SPE Res. Eng*. **1988**, 8, 1033-1040.

Khosharay, S.; Varaminian, F. Experimental and modeling investigation on surface tension and surface properties of (CH_4 + H_2O), (C_2H_6 + H_2O), (CO_2 + H_2O) and (C_3H_8 + H_2O) from 284.15K to 312,15K and pressures up to 60bar. *Int. J. Refrig*. **2014**, 47, 26-35.

King, M.B.; Mubarak, A.; Kim, J.D.; Bott, T.R. The mutual solubilities of water with supercritical and liquid carbon-dioxide. *J. Supercri. Fluids*. **1992**, 5, 296-302.

Kontogeorgis, G.M.; Voutsas, E.C.; Yakoumis, I.V.; Tassios, D.P. An equation of state for associating fluids. *Ind. Eng. Chem. Res*. **1996**, 35, 4310-4318.

Kunz, O.; Wagner, W. The GERG-2008 wide-range equation of state for natural gases and other mixtures: an expansion of GERG-2004. *J. Chem. Eng. Data*. **2012**, 57, 3032-3091.

Kvamme, B.; Kuznetsova, T.; Hebach, A.; Oberhof, A.; Lunde, E. Measurements and modelling of interfacial tension for water + carbon dioxide systems at elevated pressures. *Comput. Mater. Sci*. **2007**, 38, 506-513.

Lemmon, E.W.; McLinden, M.O.; Friend, D.G. Thermophysical properties of fluid systems, in: P.J. Linstrom, W.G. Mallard (Eds.). NIST Chemistry WebBook, NIST Standard Reference Database Number 69, National Institute of Standards and Thecnology, Gaithersburg, MD 20899, 2011.

Li, R.; Li, H. Improved three-phase equilibrium calculation algorithm for water/hydrocarbon mixtures. *Fuel*. **2019**, 244, 517-527.

Li, Z.; Dong, M.; Li, S.; Dai, L. Densities and solubilities for binary systems of carbon dioxide plus water and carbon dioxide plus brine at 59ºC and pressures to 29 MPa. *J. Chem. Eng. Data*. **2004**, 49, 1026-1031.

Liu, Y.; Li, H.; Okuno, R. Measurements and modeling of interfacial tension for CO_2/CH_4/brine systems under reservoir conditions. *Ind. Eng. Chem. Res*. **2016**, 55, 12358-12375.

Madsen, K.; Nielsen, H.B.; Tingleff, O. Methods for non-linear least squares problems, 2nd edition. Informatics and Mathematical Modelling, Technical University of Denmark, April, 2004.

Martin, J.J. Cubic equations of state—which? *Ind. Eng. Chem. Fundam*. **1979**, 18, 81-97.

Martinez, A.; Guennec, Y.L.; Privat, R.; Jaubert, J.-N.; Mathias, P.M. Analysis of the combinations of property data that are suitable for a safe estimation of consistent Twu α-Function parameters: updated parameter values for the translated-consistent tc-PR and tc-RK cubic equations of state. *J. Chem. Eng. Data*. **2018**, 63, 3980-3988.

Matheis, J.; Müller, H.; Pfitzner, M.; Hickel, S. Modeling of real fluid effects. Sonderforschungsbereich/ Transregio 40 Annual Report. 2014.

Matheis, J.; Müller, H.; Lenz, C.; Pfitzner, M.; Hickel, S. Volume translation methods for real-gas computational fluid dynamics simulations. *J. Supercrit. Fluids* **2016**, 107, 422-432.

Mathias, P.M.; Copeman, T.W. Extension of the Peng-Robinson equation of state to complex mixtures: evaluation of the various forms of the local composition concept. *Fluid Phase Equilib*. **1983**, 13, 91-108.

Michelsen, M.L. The isothermal flash problem. Part I. Stability. *Fluid Phase Equilib.* **1982**, 9, 1-19.

Nighswander, J.A.; Kalogerakis, N.; Mehrotra, A.K. Solubilities of carbon dioxide in water and 1 wt% NaCl solution at pressures up to 10 MPa and temperatures from 80 to 200°C. *J. Chem. Eng. Data*. **1989**, 34, 355-360.

Park, J.Y.; Lim, J.S.; Yoon, C.H.; Lee, C.H.; Park, K.P. Effect of a fluorinated Sodium Bis (2-ethylhexyl) sulfosuccinate (Aerosol-OT, AOT) analogue surfactant on the interfacial tension of CO_2 + water and CO_2 + Ni-Plating solution in near- and supercritical CO_2. *J. Chem. Eng. Data*. **2005**, 50, 299-308.

Pedersen, K.S.; Milter, J.; Rasmussen, C.P. Mutual solubility of water and a reservoir fluid at high temperatures and pressures: experimental and simulated data. *Fluid Phase Equilib*. **2001**, 189, 85-97.

Pereira, L.; Chapoy, A.; Burgass, R., Oliveira, M.B.; Coutinho, J.; Tohidi, B. Study of the impact of high temperatures and pressures on the equilibrium densities and interfacial tension of the carbon dioxide/water system. *J. Chem. Thernodyn*. **2016**, 93, 404-415.

Peneloux, A.; Rauzy, E.; Freze, R. A consistent correction for Redlich-Kwong-Soave volumes. *Fluid Phase Equilib*. **1982**, 8, 7-23.

Peng, D.Y.; Robinson, D.B. A new two-constant equation of state. *Ind. Eng. Chem. Fundamen*. **1976**, 15, 59-64.

Rachford Jr, H.H.; Rice, J.D. Procedure for use of electronic digital computers in calculating flash vaporization hydrocarbon equilibrium. *J. Pet. Technol*. **1952**, 410, 19-3.

Sako, T.; Sugata, T.; Nakazawa, N.; Obuko, T.; Sato, M.; Taguchi, T.; Hiaki, T. Phase equilibrium study of extraction and concentration of furfural produced in reactor using supercritical carbon dioxide. *J. Chem. Eng. Jpn*. **1991**, 24, 449-454.

Schechter, D.S.; Guo, B. Parachors based on modern physics and their uses in IFT prediction of reservoir fluids. *SPE Res. Eval. Eng*. **1998**, 1, 207-217.

Shariat, A.; Moore, R.G.; Mehta, S.A.; Fraassen, K.C.; Newsham, K.E.; Rushing, J.A. Laboratory measurements of CO_2-H_2O interfacial tension at HP/HT conditions: implications for CO_2 sequestration in deep aquifers. Paper CMTC 150010 presented at Carbon Management Technology Conference. Orlando, Florida, USA, February 7-9, 2012.

Soave, G. Equilibrium constants from a modified Redlich-Kwong equation of state. *Chem. Eng. Sci*. **1972**, 27, 1197-1203.

Song, K.Y.; Kobayashi, R. Water content of CO_2 in equilibrium with liquid water and/or hydrates. *SPE Form. Eval*. **1987**, 2, 500-508.

Song, Y.; Chen, C. Symmetric electrolyte nonrandom two-liquid activity coefficient model. *Ind. Eng. Chem. Res*. **2009**, 48, 7788-7797.

Søreide, I.; Whitson, C. Peng-Robinson predictions for hydrocarbons, CO_2, N_2, and H_2S with pure water and NaCl brine. *Fluid Phase Equilib*. **1992**, 77, 217-240.

Sørensen, H.; Pedersen, K.; Christensen, P. Modeling of gas solubility in brine. *Org. Geochem*. **2002**, 33, 635-642.

Spycher, N.; Pruess, K.; King, J.E. CO_2-H_2O mixtures in the geological sequestration of CO_2. I. Assessment and calculation of mutual solubilities from 12 to 100°C and up to 600 bar. *Geochim. Cosmochim. Ac*. **2003**, 67, 3015-3031.

Stryjek, R.; Vera, J.H. PRSV: an improved Peng-Robinson equation of state for pure compounds and mixtures. *Can. J. Chem. Eng*. **1986**, 64, 323-333.

Sugden, S. The Parachors and valency. 1930.

Tabasinejad, F.; Barzin, Y.; Moore, G.R.; Mehta, S.A.; Fraassen, K.C.V.; Rushing, J.A.; Newsham, K.E. Water/CO_2 system at high pressure and temperature conditions: measurement and modeling of density in equilibrium liquid and vapor phases. Paper SPE 131636 presented at the SPE EUROPEC/EAGD Annual Conference and Exhibition. Barcelona, Spain, June 14-17, 2010.

Teng, H.; Yamasaki, A.; Chun, M.K.; Lee, H. Solubility of liquid CO_2 in water at temperatures from 278 K to 293 K and pressures from 6.44 MPa to 29.49 MPa and densities of the corresponding aqueous solutions. *J. Chem. Thermodyn*. **1997**, 29, 1301-1310.

Tödheide, K.; Frank, E.U. Das Zweiphasengebiet und die kritische Kurve im system kohlendioxid-wasser bis zu drucken von 3500 bar. *Z. Phys. Chemie*. **1962**, 37, 387-401.

Trusler, J.P.M. Thermophysical properties and phase behavior of fluids for application in carbon capture and storage processes. *Annu. Rev. Chem. Biomol. Eng*. **2017**, 8, 381-402.

Twu, C.H.; Bluck, D.; Cunningham, J.R.; Coon, J.E. A cubic equation of state with a new alpha function and a new mixing rule. *Fluid Phase Equilib*. **1991**, 69, 33-50.

Valtz, A.; Chaopy, A.; Coquelet, C.; Paricaud, P.; Richon, D. Vapor-liquid equilibria in the carbon dioxide-water system, measurement and modeling from 278.2 to 318.2 K. *Fluid Phase Equilib*. **2004**, 226, 333-344.

van der Waals, J.D. Continuity of the gaseous and liquid state of matter. 1873.

Weibe, R.; Gaddy, V.L. The solubility in water of carbon dioxide at 50, 75, and 100^o, at pressures to 700 atmospheres. *J. Am. Chem. Soc*. **1939**, 61, 315-318.

Weibe, R.; Gaddy, V.L. The solubility of carbon dioxide in water at various temperatures from 12 to 40^o and at pressures to 500 atmospheres: critical phenomena. *J. Am. Chem. Soc.* **1940**, 62, 815-817.

Wilson, G.M.A modified Redlich-Kwong equation of state, application to general physical data calculations. Paper 15c presented at the AIChE Natl. Meeting. Cleveland, Ohio, USA, 1969.

Whitson, C.H.; Brulé, M.R. Phase behavior (vol. 20). Richardson, TX: Henry L. Doherty Memorial Fund of AIME. *SPE*. **2000**.

Wong, D.S.H; Sandler, S.I. A theoretically correct mixing rule for cubic equations of state. *AIChE J*. **1992**, 38, 671-680.

Yaginuma. R.; Sato. Y.; Kodama, D.; Tanaka, H.; Kato, M. Saturated densities of carbon dioxide + water mixture at 304.1 K and pressures to 10 MPa. *J. Jpn. Instit. Energy*. **2000**, 79, 144-146.

Yan, Y.; Chen, C. Thermodynamic modeling of CO_2 solubility in aqueous solutions of NaCl and Na_2SO_4. *J. Supercrit. Fluids*. **2010**, 55, 623-634.

Young, A.F.; Pessoa, F.L.P.; Ahón, V.R.R. Comparison of volume translation and co-volume functions applied in the Peng-Robinson EoS for volumetric corrections. *Fluid Phase Equilib*. **2017**, 435, 73-87.

Zhang, J.; Feng, Q.; Wang, S.; Zhang, X.; Wang, S. Estimation of CO_2-brine interfacial tension using an artificial neural network. *J. Supercrit. Fluids* **2016**, 107, 31-37.

Zhao, H.; Lovo, S.N. Phase behavior of the CO_2-H_2O system at temperatures of 273-623 K and pressures of 0.1-200 MPa using Peng-Robinson-Stryjek-Vera equation of state with a modified Wong-Sandler mixing rule: an extension to the CO_2-CH_4-H_2O system. *Fluid Phase Equilib*. **2016**, 417, 96-108.

APPENDIX

Appendix A. Derivation of activity coefficient in the fugacity expression when Huron-Vidal mixing rule is used.

Similar to the approach used by Wong and Sandler (Wong and Sandler, 1992), the activity coefficient of component *i* can be expressed by the following formula:

$$\ln\gamma_i = \frac{1}{RT}\frac{\partial G_\infty^E}{\partial z_i} \tag{A1}$$

where excess Gibbs free energy can be expressed as (Huron and Vidal, 1979):

$$G_\infty^E = RT\sum_{i=1}^{n} z_i \frac{\sum_{j=1}^{n}\tau_{ji}b_j z_j \exp\left(-\alpha_{ji}\tau_{ji}\right)}{\sum_{k=1}^{n} b_k z_k \exp(-\alpha_{ki}\tau_{ki})} \tag{A2}$$

To make the derivation process more intuitive, we can set $i = 1$ (the first component) and $n = 2$ (two compounds in the system). And the partial derivative becomes:

$$\frac{1}{RT}\frac{\partial G_\infty^E}{\partial z_1} = z_1 \cdot \frac{\sum_{j=1}^{n}\tau_{j1}b_j z_j \exp\left(-\alpha_{j1}\tau_{j1}\right)}{\sum_{k=1}^{n} b_k z_k \exp(-\alpha_{k1}\tau_{k1})} + z_2 \cdot \frac{\sum_{j=1}^{n}\tau_{j2}b_j z_j \exp\left(-\alpha_{j2}\tau_{j2}\right)}{\sum_{k=1}^{n} b_k z_k \exp(-\alpha_{k2}\tau_{k2})} \tag{A3}$$

After taking the partial derivative, the first part of **Equation (A3)** can be written as:

$$\begin{aligned}
&\frac{\partial}{\partial z_1}\left(z_1 \cdot \frac{\sum_{j=1}^{n}\tau_{j1}b_j z_j \exp\left(-\alpha_{j1}\tau_{j1}\right)}{\sum_{k=1}^{n} b_k z_k \exp(-\alpha_{k1}\tau_{k1})}\right) \\
&\qquad = \frac{\sum_{j=1}^{n}\tau_{j1}b_j z_j \exp\left(-\alpha_{j1}\tau_{j1}\right)}{\sum_{k=1}^{n} b_k z_k \exp(-\alpha_{k1}\tau_{k1})} + z_1 \\
&\qquad \cdot \left(\frac{\tau_{11}b_1 \exp(-\alpha_{11}\tau_{11}) \cdot \left(\sum_{k=1}^{n} b_k z_k \exp(-\alpha_{k1}\tau_{k1})\right)}{\left(\sum_{k=1}^{n} b_k z_k \exp(-\alpha_{k1}\tau_{k1})\right)^2}\right. \\
&\qquad \left. - \frac{b_1 \exp(-\alpha_{11}\tau_{11}) \cdot \left(\sum_{j=1}^{n}\tau_{j1}b_j z_j \exp\left(-\alpha_{j1}\tau_{j1}\right)\right)}{\left(\sum_{k=1}^{n} b_k z_k \exp(-\alpha_{k1}\tau_{k1})\right)^2}\right)
\end{aligned} \tag{A4}$$

and the second part of **Equation (A3)** becomes:

$$\frac{\partial}{\partial z_1}\left(z_2 \cdot \frac{\sum_{j=1}^{n} \tau_{j2} b_j z_j \exp\left(-\alpha_{j2}\tau_{j2}\right)}{\sum_{k=1}^{n} b_k z_k \exp(-\alpha_{k2}\tau_{k2})}\right)$$

$$= z_2$$

$$\cdot \left(\frac{\tau_{12} b_1 \exp(-\alpha_{12}\tau_{12}) \cdot (\sum_{k=1}^{n} b_k z_k \exp(-\alpha_{k2}\tau_{k2}))}{(\sum_{k=1}^{n} b_k z_k \exp(-\alpha_{k2}\tau_{k2}))^2}\right. \tag{A5}$$

$$\left. - \frac{b_1 \exp(-\alpha_{12}\tau_{12}) \cdot \left(\sum_{j=1}^{n} \tau_{j2} b_j z_j \exp\left(-\alpha_{j2}\tau_{j2}\right)\right)}{(\sum_{k=1}^{n} b_k z_k \exp(-\alpha_{k2}\tau_{k2}))^2}\right)$$

As such, **Equation (A1)** can be expressed as:

$$\frac{1}{RT}\frac{\partial G_{\infty}^{E}}{\partial z_1} = \frac{\sum_{j=1}^{n} \tau_{j1} b_j z_j \exp\left(-\alpha_{j1}\tau_{j1}\right)}{\sum_{k=1}^{n} b_k z_k \exp(-\alpha_{k1}\tau_{k1})} + \frac{z_1 b_1 \exp(-\alpha_{11}\tau_{11})}{\sum_{k=1}^{n} b_k z_k \exp(-\alpha_{k1}\tau_{k1})}$$

$$\cdot \left(\tau_{11} - \frac{\sum_{j=1}^{n} \tau_{j1} b_j z_j \exp\left(-\alpha_{j1}\tau_{j1}\right)}{\sum_{k=1}^{n} b_k z_k \exp(-\alpha_{k1}\tau_{k1})}\right)$$

$$+ \frac{z_2 b_1 \exp(-\alpha_{12}\tau_{12})}{\sum_{k=1}^{n} b_k z_k \exp(-\alpha_{k2}\tau_{k2})} \tag{A6}$$

$$\cdot \left(\tau_{12} - \frac{\sum_{j=1}^{n} \tau_{j2} b_j z_j \exp\left(-\alpha_{j2}\tau_{j2}\right)}{\sum_{k=1}^{n} b_k z_k \exp(-\alpha_{k2}\tau_{k2})}\right)$$

Using letter *i* to replace number 1 leads to a general expression for activity coefficient (Huron and Vidal, 1979):

$$\ln\gamma_i = \frac{1}{RT}\frac{\partial G_\infty^E}{\partial z_i}$$

$$= \frac{\sum_{j=1}^{n} \tau_{ji} b_j z_j \exp\left(-\alpha_{ji}\tau_{ji}\right)}{\sum_{k=1}^{n} b_k z_k \exp\left(-\alpha_{ki}\tau_{ki}\right)}$$

$$+ \sum_{j=1}^{n}\left[\frac{b_i z_j \exp\left(-\alpha_{ij}\tau_{ij}\right)}{\sum_{k=1}^{n} b_k z_k \exp\left(-\alpha_{kj}\tau_{kj}\right)}\right. \tag{A7}$$

$$\left.\cdot\left(\tau_{ij} - \frac{\sum_{l=1}^{n} \tau_{lj} b_l z_l \exp\left(-\alpha_{lj}\tau_{lj}\right)}{\sum_{k=1}^{n} b_k z_k \exp\left(-\alpha_{kj}\tau_{kj}\right)}\right)\right]$$